ISTANBUL TECHNICAL UNIVERSITY ★ GRADUATE SCHOOL OF SCIENCE ENGINEERING AND TECHNOLOGY

QUATERNARY AMMONIUM SALT CONTAINING ANTIBACTERIAL NANOFIBERS

M.Sc. THESIS

Nurullah UYKUN

Department of Chemistry

Chemistry Programme

May 2014

ISTANBUL TECHNICAL UNIVERSITY ★ GRADUATE SCHOOL OF SCIENCE ENGINEERING AND TECHNOLOGY

QUATERNARY AMMONIUM SALT CONTAINING ANTIBACTERIAL NANOFIBERS

M.Sc. THESIS

Nurullah UYKUN
(509121023)

Department of Chemistry

Chemistry Programme

Thesis Advisor: Prof. Dr. A. Sezai SARAC

May 2014

İSTANBUL TEKNİK ÜNİVERSİTESİ ★ FEN BİLİMLERİ ENSTİTÜSÜ

KUATERNER AMONYUM TUZU İÇEREN ANTİBAKTERİYEL NANOFİBERLER

YÜKSEK LİSANS TEZİ

Nurullah UYKUN
509121023

Kimya Bölümü

Kimya Programı

Tez Danışmanı: Prof. Dr. A. Sezai SARAÇ

Mayıs 2014

Nurullah UYKUN, a **M.Sc.** student of ITU **Institute of Science, Technology and Engineering of** student ID **509121023**, successfully defended the **thesis/dissertation** entitled "**QUATERNARY AMMONIUM SALT CONTAINING ANTIBACTERIAL NANOFIBERS**", which he prepared after fulfilling the requirements specified in the associated legislations, before the jury whose signatures are below.

Thesis Advisor :	**Prof. Dr. A. Sezai SARAC** İstanbul Technical University	.....
Jury Members :	**Prof. Dr. Yücel ŞAHİN** Yıldız Technical University	.....
	Prof. Dr. Ahmet AKAR İstanbul Technical University	.....

Date of Submission : 5 May 2014
Date of Defense : 26 May 2014

To my family,

FOREWORD

I would like to express my gratitude to my thesis supervisor, Prof. Dr. A.Sezai SARAÇ for his continuous encouragement, guidance, helpful critics and discussions in my studies.

First, I would like to say that I appreciate Dr. Argun T. GÖKÇEÖREN for his limitless help and informations, encouragement and guidance, and his supports in both my academic and normal life. I would like to give my special thanks to my laboratory friends; Mehmet Giray ERSÖZOĞLU, Burcu SAYINLI, Aslı GENÇTÜRK, Timuçin BALKAN, Mehmet Tolga SATICI, Dilek Suadiye, Ömer EROĞLU, Uğur DAĞLI, Yahya TOPRAK, Keziban HÜNER, İlknur GERGİN, Zeliha GÜLER and Diğdem GİRAY AYTAÇ for their collaborative and friendly manner.

Furthermore, I am glad to work on this collaborative project with Doc. Dr. Burçak KARAGÜZEL KAYAOĞLU, Yrd. Doc. Dr. İkilem GÖCEK from Department of Textile Engineering and Doc. Dr. Alper T. AKARSUBAŞI from Department of Molecular Biology and Genetics. I am thankful for their collaborations and supports during my master survive.

Most of all, I would like to thank my family, my father Ahmet UYKUN, my mother Sevilay UYKUN and my brother Selim UYKUN. In particular, I would like to attribute to my lifes' special person, my fiance Özlem ALASAĞ. For all those times, they supported me to surpass every obstacle in my life. I was able to achieve everything in my life thanks to their sincere love.

Finally, I would like to thank all of my other friends for all their emotional assists and motivation during this extremely difficult accomplishment.

May 2014

Nurullah UYKUN
Chemist

TABLE OF CONTENTS

Page

ABBREVIATIONS

AFM : Atomic Force Microscopy

Ag : Silver

AgBr : Silver bromide

$AgNO_3$/PAN : Silver nitrate and Polyacrylonitrile

CPC : Cetylpyrridinium chloride

CTAB : Cetyltrimethylammonium bromide

DMF : Dimethylformamide

EIS : Electrochemical Impedance Spectroscopy

E.coli : Escherichia coli

FTIR-ATR : Fourier Transform Infrared Spectroscopy-Attenuated Total Reflectance

ITO : Indium tin oxide

K.pneumonia: Klebsiella pneumonia

PBS : Phosphate buffer solution

PVP : Polyvinylpyrrolidone

PVP/CPC : Polyvinylpyrrolidone fibers incorporated with cetylpyrridinium chloride

PVP/CTAB : Polyvinylpyrrolidone fibers incorporated with cetyltrimethylammonium bromide

S.aureus : Staphylococcus aureus

SEM : Scanning Electron Microscopy

TiO_2 : Titanium dioxide

TiO_2/PVA : Titanium dioxide and Polyvinylalcohol

UV-Vis : Ultraviole Visible

LIST OF TABLES

Page

LIST OF FIGURES

Page

QUATERNARY AMMONIUM SALT CONTAINING ANTIBACTERIAL NANOFIBERS

SUMMARY

Different techniques have been used in the preparation of nanoscale structures with a high surface area such as biomaterial scaffolds for vascular grafts, wound dressings or air purifying filters. In the present study, an antibacterial agent, such as cethyltrimethyl ammonium bromide(CTAB) and cetylpyrridinum chloride (CPC) have been incorporated into the nanofibers by using electrospinning to prepare a nanofibrous material with an antibacterial efficacy for a potential wound healing application. Polyvinylpyrrolidone (PVP) known as a biocompatible additive in food and drug industries, has been used as fiber processing agent with the organic active ingredients, CTAB and CPC. Different weight ratios (%wt/vol) of PVP/CTAB and PVP/CPC blends were prepared and successfully electrospun. The morphology and electroactive characters of the nanofibers were investigated by scanning electron microscopy (SEM), atomic force microscopy (AFM) and electrochemical impedance spectroscopy (EIS). Fiber diameters and charge transfer resistances were found to decrease with salt content, while the antibacterial activity and the double layer capacitance increased with no apparent effect on the specific capacitance providing favorable conditions for the fabrication of biomaterials.

KUATERNER AMONYUM TUZU İÇEREN ANTİBAKTERİYEL NANOFİBERLER

ÖZET

Birçok farklı teknik, yara bantları, hava filtreleri veya organ nakilleri için biyomateryal malzemeler gibi geniş yüzey alanına sahip nanoboyutta yapıların hazırlanılması için kullanılmaktadır. Bu çalışmada, cetyltrimethyl amonyum bromür (CTAB) ve cetylpyrridinium klorür (CPC) gibi antibakteriyel özellik gösteren quaterner amonyum tuzları, antibakteriyel aktivitesi yüksek yara iyileştirici membran uygulamalarında çalışılmak üzere nano gözenekli malzeme elde etmek için kullanılmıştır. Gıda ve ilaç endüstrilerinde sıkça kullanılan polivinilpirolidon (PVP) biyobozunur bir polimer olup, bu çalışmada organik kuaternize amonyum tuzları (CTAB ve CPC) taşıyan fiberler elde edilmek üzere kullanılmıştır. Farklı oranlarda PVP/CTAB ve PVP/CPC karışımları hazırlanarak başarıyla fiberleri oluşturulmuştur. Hazırlanan bu fiberlerin morfolojik özellikleri taramalı electron mikroskobu (SEM) ve atomik kuvvet mikroskobu (AFM) ile, elektroaktif özellikleri elektrokimyasal empedans spekroskopisi (EIS) ile, optik özellikleri UV-görünür bölge spektroskopisi ve fourier dönüşümlü kızılötesi spektroskopisi (FTIR) ile karakterize edilmiştir.

PVP/CTAB ve PVP/CPC ye ait SEM analizleri incelendiğinde; organik kuaternize amonyum tuzu katılmamış PVP fiberleri, tuz ile kompozit oluşturan PVP fiberlerine göre daha homojen ve pürüzsüz bir yüzeye sahiptir. Fakat tuz ilave edilmemiş PVP fiberleri, tuz ilave edilen fiberlere göre daha kalındır. SEM görüntülerinden elde edilen 50 farklı fiberin çapları ölçülerek ortalama bir değer elde edildiğinde görülmektedir ki, artan tuz miktarlarında fiber çapı azalan bir eğilim göstermektedir.

AFM sonuçları ise bize yüzeyin ne kadar pürüzlü olduğunu göstermektedir. Tuz ilave edilmemiş PVP fiberleri, daha pürüzsüz ve homojen olduğunu bu analiz sonucunda alınan değerlerle ispatlamıştır. Artan miktarlarda ilave edilen tuz ile oluşturulan fiberlerin pürüzlülüğünün daha fazla olduğu açıkça belirtilmiştir.

FTIR ile yapılan yüzey analizinde, PVP için karakteristik olan C=O ve C-N pikleri, sırasıyla 1655 cm^{-1} ve 1285 cm^{-1} dalgaboyunda görülmekte olup, CTAB ve CPC nin uzun alkil gruplarının verdiği C-H piki ise 2900 cm^{-1} civarında kendini göstermektedir.

Bu çalışmada, UV-görünür bölge ve elektrokimyasal empedans spektroskopisi analizlerini gerçekleştirmek amacıyla suda veya organik çözücülerde çözünmeyen veya kısmen daha az çözünen çapraz bağlı PVP elde edildi. Çapraz bağlı polivinilpolipirolidon (PVPP) elde etmek için elektrospinning ile elde edilen nanofiberler 150 ^{o}C de 24 saat boyunca etüvde tutuldu. Bu örneklerden alınan FTIR spektrumlarına bakıldığında PVP ye ait C=O pikinin giderek yok olmaya başladığı ve hemen yanında 1700 cm^{-1} lerde yeni bir pik oluştuğu gözlenmektedir.

UV-görünür bölge spektroskopisi ile PVP ile yüksek miktardaki tuzun oluşturduğu fiber üzerinden 1 haftalık salınımı incelenmiştir. Alınan sonuçlarda, Brom iyonlarına ait pik 275 nm de görüşmüş olup, 2. günde salınımının tamamını gerçekleştirdiği ve daha sonra sabit kaldığı gözlenmiştir.

Elektrokimyasal empedans spektroskopisi analizi ile ilave edilen tuz miktarının iletkenliği ne kadar değiştirdiği ve bunun sonucunda fiber çapına yaptığı etki ve antibakteriyel aktivitesi tartışılmıştır. Empedans ölçümleri yapabilmek amacıyla ITOPET üzerinde nanofiberler oluşturulmuş ve fosfat tampon çözeltisinde çözünmeyen fiberler elde etmek amacıyla etüvde ısıtılarak PVP'nin çapraz bağlanması sağlanmıştır. Nyquist, Bode magnitude ve Bode phase diyagramlarından görülebileceği üzere, tuz miktarı arttıkça direnç 90000 ohm dan 40000 ohm a düşmekte, dolayısıyla kapasitif özellik artmaktadır. Faz açısı ise 60-80^{o} arasında değişmektedir.

Antibakteriyel aktiviteyi belirlemek amacıyla, farklı tuz miktarları ilave edilerek elde edilen PVP nanofiberleri, üç farklı bakteri kullanılarak test edildi, Klebsiella pneumonia ATCC 4352, Escherichia coli ATCC 10536 and S. aureus ATCC 6538. ISO 20743:2007 standartlarına göre kantitatif sayım metodu uygulamak üzere dört farklı orandaki PVP/CTAB nanofiberleri ile kontrol amaçlı PVP nanofiberi test edildi. Elde edilen sonuçlara göre, %1 lik tuz miktarı bile standartları karşılamak için yeterlidir. Ayrıca, CTAB/PVP oranı yüksek olan son üç örnek, bakterilerin üremesini engellemek ve onları yok etmek için oldukça yüksek antibakteriyel aktiviteye sahiptir.

Fiber çapları ve yük transfer direnci artan tuz miktarlarında azalmakla birlikte, antibakteriyel aktivite ve double layer kapasitans artmaktadır. Bunun yanında spesifik kapasitans da önemli bir değişim gözlenmemiştir. Biyomateryallerin fabrikasyonu için en uygun koşullar sağlanmış olup, karakterizasyonları başarıyla tamamlanmıştır.

1. INTRODUCTION

Different techniques have been used to compose inorganic nanoparticles with a polymer matrix such as sol-gel processing, dip-coating, spin-coating, and evaporation–deposition. Nowadays, composite nanofiber materials obtained by blending organic-inorganic nanoparticles have attracted great interest for the purpose of creating new materials with enhanced mechanical, thermal, optical, electrical, antimicrobial, antifouling and catalytic properties [1].

Many processing techniques, such as drawing [2], template synthesis [3], phase separation [4], self-assembly [5] and electrospinning [6-7], have been used to produce polymeric nanofibers. Electrospinning has the advantage as a simple and low cost method that uses electrostatic forces for producing fibers with diameters in the nanometer to micron range. A high-voltage power supply generates an electric field between a syringe and a grounded collector. Electrostatic charging of the fluid at the tip of the nozzle results in the formation of the Taylor cone, from the apex of which a single fluid jet is ejected. As the charged jet travels to the collector, it readily dries out, forming nonwoven fibrous mats depositing on the collector [1,4,8].

Nanofibrous webs have the advantage due to their high surface area to volume ratio of the nanofibers. Nanofibrous mats have been found to have high antibacterial effectiveness which creates potential uses to them as high-performance filters, protective textiles, biomedical devices, wound dressings, hospital beddings, medical clothing for hospital staff, sports clothing, shoe linings, arm bands, sleeping bags and toys for children, also for hygienic under-wears as well as ladies tights [1,2,6,8,9,10].

Recently active ingredients, such as therapeutic compounds, antimicrobials and antibiotics were incorporated in electrospun nanofibers, because the nanofiber webs have very strong efficacy of the drug due to their high surface area-to-volume ratio and controlled release of the activity. The other ingredients of high importance in various biomedical fields such as wound dressing materials, body wall repairs, augmentation devices, tissue scaffolds, antimicrobial filters, are silver (Ag) ions, silver compounds and silver salts [11,12,13,14,15]. For preventing bacterial

attachment and biofilm formation on the surfaces, application of surface coatings, or modification and/or alteration of the surface structure have been utilized [16].

Lee et al. reported the antimicrobial activity of the $AgNO_3$/PAN precursor solution against gram positive Staphylococcus aureus ATCC 6538 and gram negative Escherichia coli (E. coli) ATCC 25922 [4]. Wu et al. developed antibacterial membranes with multicomponent system containing Ag, AgBr, TiO_2 and hydroxyapatite as four active components to achieve more efficient antibacterial activity [5]. Sheikh et al. developed polyurethane nanofiber webs containing silver nanoparticles using the electrospinning technique. They also studied the stability of nanoparticles after many washing cycles and recommended the use of electrospun nanofiber mats in water purifying systems [6]. Pant et al. developed electrospun nylon-6 nanofiber mats containing TiO_2 nanoparticles for water filter applications. The incorporation of TiO_2 nanoparticles in nylon-6 solution was found to improve the hydrophilicity, mechanical strength, antimicrobial and UV protecting ability of electrospun webs [1]. Lee et al. reported on the ultraviolet protective and antibacterial properties of electrospun TiO_2/PVA nano fiber web as a multifunctional textile nanocomposite material [17].

As the quaternary ammonium content of a polymer increases, because of the increased charge density of the polymeric solution needed for the electrospinning process, the average diameter sizes of the electrospun polymers decreases. In addition to providing antibacterial efficacy for electrospun mats, this is also another positive impact of quaternary ammonium group on the polymers processed with electrospinning [18].

Due to its biocompatibility and nontoxic nature, polyvinyl pyrrolidone, PVP, a synthetic, water soluble polymer, finds applications in biomedical fields such as a blood plasma expander and a vitreous humor substitute [3,19,20]. Since polyvinylpyrrolidone (PVP) is a water-soluble polymer, it has been used for controlled release of drugs by the oral route [21,22,23], also in pharmacy as a protective colloid, viscosity-enhancing agent, solubility promoter, granulating, tabletting agent, and film-forming material [24,25].

The UV cured film of n-vinyl pyrrolidone have been used as a potential bioadhesive wound dressing matrix when blended with other polymeric materials [3]. In the work of Singh et al., skin covers and wound dressings made of Poly(vinyl alcohol) (PVA) and poly(N-vinylpyrrolidone) (PVP) were produced with or without polysaccharides

by the help of gamma irradiation technique. Because of its biocompatibility and nontoxicity, PVP was also chosen as the base material for the drug-loading device. Drug release from this membrane was found to depend on the cross-linking density, composition and membrane thickness [26]. On the other hand, PVP has been used as carrier on electrospun fibers application [8].

In the current study, a novel antibacterial nanofibrous membrane was prepared by electrospinning of polyvinyl pyrrolidone (PVP)/cethyltrimethyl ammonium bromide (CTAB) salt aqueous solution into nanofibrous webs. The individual features of PVP and quaternary ammonium compound (cethyltrimethyl ammonium bromide (CTAB) or cetylpyrridinum chloride (CPC)) have inspired us to utilize them to develop an effective material for wound healing application.

This work pursued to fabricate an effective wound healing substance because the basic material, PVP, is water-soluble, biocompatible biopolymer and the active ingredient (CTAB or CPC) is an organic material. It also has a potential drug release capacity due to its hydrophilic properties. The nanofibrous web structure of the PVP membrane provides a large surface area to absorb water molecules, which potentially increases the drug dissolution rate [23].

In this study, three different bacteria with gram-postive and gram-negative characteristics were used. Klebsiella pneumonia, ATCC 4352 [27,28], Escherichia coli, ATCC 10536 [29] and S. aureus ATCC 6538 [30], were selected to determine the antimicrobial activity of nanofibrous webs made from polyvinyl pyrrolidone (PVP)/cethyltrimethylammonium bromide (CTAB) salt aqueous solutions. Also a very detailed chemical characterization was performed on the produced nanofibrous webs by carrying out Fourier transform Infrared Spectroscopy (FTIR), UV-Vis and Electrochemical Impedance Spectroscopy (EIS) measurements.

2. THEORETICAL PART

2.1. Material

2.1.1 Poly vinylpyrrolidone

Polyvinylpyrrolidone (PVP), also commonly called polyvidone or povidone, is a water-soluble polymer made from the monomer N-vinylpyrrolidone [31].

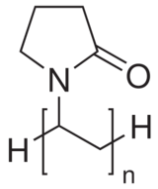

Figure 2.1: General formula of PVP.

It is used as a binder in many pharmaceutical tablets; [32] it simply passes through the body when taken orally. However, autopsies have found that crospovidone (PVPP) contributes to pulmonary vascular injury in substance abusers who have injected pharmaceutical tablets intended for oral consumption [33]. The long-term effects of crospovidone or povidone within the lung are unknown.

PVP added to iodine forms a complex called povidone-iodine that possesses disinfectant properties. This complex is used in various products like solutions, ointment, pessaries, liquid soaps and surgical scrubs. It is known under the trade name Betadine and Pyodine.

It is used in pleurodesis (fusion of the pleura because of incessant pleural effusions). For this purpose, povidone iodine is equally effective and safe as talc, and may be preferred because of easy availability and low cost [34].

2.1.2 Quaternary ammonium cations

Quaternary ammonium cations are positively charged polyatomic ions of the structure NR_4^+, R being an alkyl group or an aryl group [35]. Unlike the ammonium ion (NH_4^+) and the primary, secondary, or tertiary ammonium cations, the quaternary

ammonium cations are permanently charged, independent of the pH of their solution. Quaternary ammonium salts or quaternary ammonium compounds (called quaternary amines) are salts of quaternary ammonium cations with an anion.

Quaternary ammonium compounds are prepared by alkylation of tertiary amines, in a process called quaternization [36]. Typically one of the alkyl groups on the amine is larger than the others. A typical synthesis is for benzalkonium chloride from a long-chain alkyldimethylamine and benzyl chloride:

$$CH_3(CH_2)_nN(CH_3)_2 + ClCH_2C_6H_5 \rightarrow [CH_3(CH_2)_nN(CH_3)_2CH_2C_6H_5]^+Cl^-$$

Figure 2.2: Synthesis of quaternary ammonium cations.

Quaternary ammonium salts have utilization areas as disinfectants, surfactants, fabric softeners, and as antistatic agents (e.g. in shampoos). The chloride salts are often used in liquid fabric softeners; however, the sulfate salts are often used in dryer anticling strips. Quaternary ammonium compounds have been proved that they have antimicrobial activity [37]. Certain quaternary ammonium compounds, especially those containing long alkyl chains, are used as antimicrobials and disinfectants. Examples are benzalkonium chloride, benzethonium chloride, methylbenzethonium chloride, cetalkonium chloride, cetylpyridinium chloride, cetrimonium, cetrimide, tetraethylammonium bromide, didecyldimethylammonium chloride and domiphen bromide. They have also shown good activity against fungi, amoeba, and enveloped viruses, quats act by disrupting the cell membrane. Quaternary ammonium compounds are lethal to a wide variety of organisms except endospores, such as Mycobacterium tuberculosis and non-enveloped viruses.

In contrast to phenolics, quaternary ammonium compounds are not very effective in the presence of organic compounds. Nonetheless, they are very effective in combination with phenols. Quaternary ammonium compounds are deactivated by soaps, other anionic detergents, and cotton fibers. But, they are not recommended for use in hard water. Effective levels are at 200 ppm and they are effective at temperatures up to 100 °C.

In organic synthesis, quaternary ammonium salts are employed as phase transfer catalysts (PTC). Such catalysts accelerate reactions between reagents dissolved in

immiscible solvents. The highly reactive reagent dichlorocarbene is generated via PTC by reaction of chloroform and sodium hydroxide.

2.1.2.1 Cetyltrimethylammonium bromide

Cetyltrimethylammonium bromide ($(C_{16}H_{33})N(CH_3)_3Br$, cetrimonium bromide, hexadecyltrimethylammonium bromide, CTAB) is one of the components of the topical antiseptic cetrimide[38]. The cetrimonium (or hexadecyltrimethylammonium) cation is an effective antiseptic agent against bacteria and fungi.

It is a cationic surfactant. Its utilization areas in industry: buffer solution for the extraction of DNA, synthesis of gold nanoparticles (e.g., spheres, rods, bipyramids), hair conditioning products.

As any surfactant, it forms micelles in aqueous solutions. At 30 °C it forms micelles with aggregation number 75-120 (depending on method of determination, usually average ~95) and degree of ionization α (fractional charge) 0.2–0.1 (from low to high concentration).

The standard constant of Br^- counterion binding to the micelle at 30 °C. This value is calculated from Br- and CTA+ ion selective electrode measurements and conductometry data by using literature data for micelle size (r = ~3 nm), extrapolated to the critical micelle concentration of 1 mM. However, it varies with total surfactant concentration so it is extrapolated to the point at which the concentration of micelles is zero).

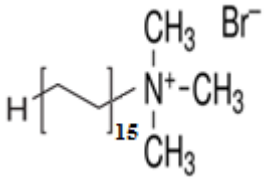

Figure 2.3: Chemical structure of CTAB.

2.1.2.2 Cetylpyridinium chloride (CPC)

Cetylpyridinium chloride (CPC) is a cationic quaternary ammonium compound used in some types of mouthwashes, toothpastes, lozenges, throat sprays, breath sprays, and nasal sprays. It is an antiseptic that kills bacteria and other microorganisms. It has been shown to be effective in preventing dental plaque and reducing gingivitis [39]. It has also been used as an ingredient in certain pesticides. Cetylpyridinium chloride may cause brown stains between the teeth and on the surface of teeth.

However, these stains can be easily removed by a dental hygienist during a routine check-up.

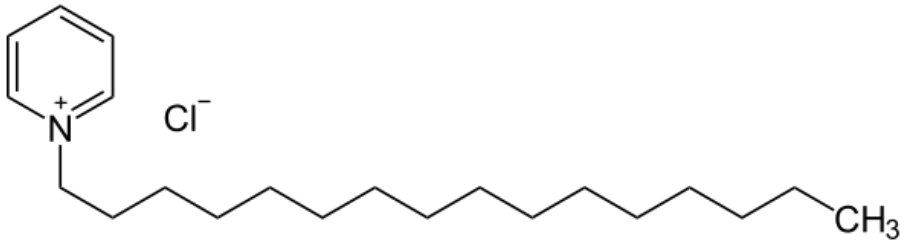

Figure 2.4: Chemical structure of CPC

2.2 Nanofiber

Nano-scaled materials have been of extensive attention on account of their many advantages, extraordinary high surface area per unit mass (for example, nanofibers with ~100 nm diameter have a specific surface of ~1000m2/g), showing Figure 2.5, coupled with high porosity, good structural mechanical properties, high axial strength combined with extreme flexibility, low basis weight, and cost effectiveness, among others [40].

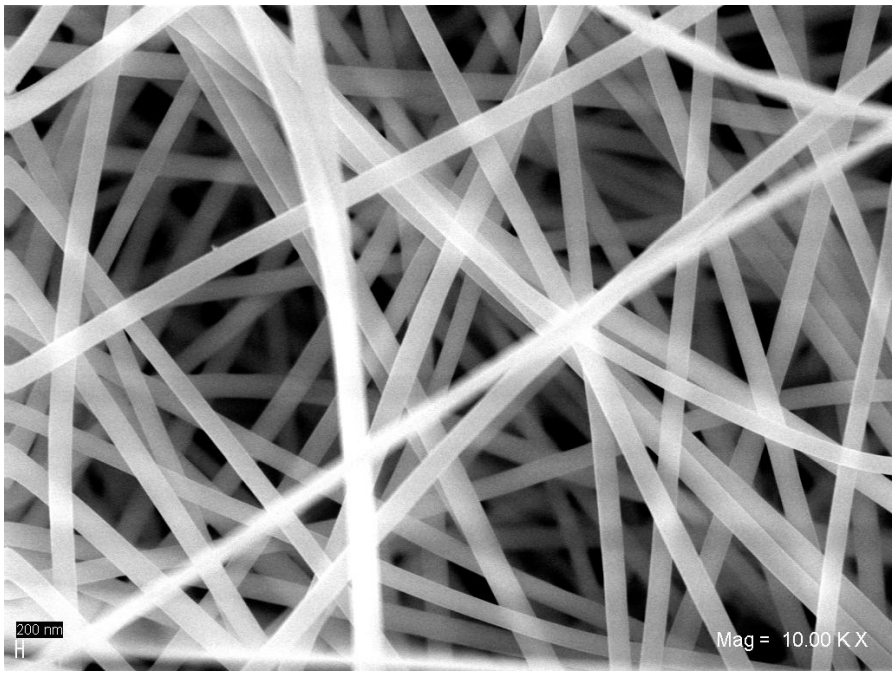

Figure 2.5: SEM image of PVP nanofibers

Fascinating point of nanofibers is that it is easily possible to modify not only their morphology and their content but also the surface structure to bear various functionalities [41,42].

2.3 Electrospinning

Electrospinning is a straightforward and cost-effective method to produce novel fibers with diameters in the range of from less than 3 nm to over 1 mm, which overlaps contemporary textile fiber technology. Electrified jets of polymer solutions and melts were investigated as routes to the manufacture of polymer nanofibers (Baumgarten, 1971; Larrondo and Manley, 1981a–c; Reneker and Chun, 1996). Since 1934, when a U.S. patent on electrospinning was issued to Formhals (1934), over 30 U.S. patents have been issued.

Nanofibers of polymers were electrospun by creating an electrically charged jet of polymer solution at a pendant or sessile droplet. In the electrospinning process a pendant drop of fluid (a polymer solution) becomes unstable under the action of the electric field, and a jet is issued from its tip. An electric potential difference, which is of the order of 10 kV, is established between the surface of the liquid drop (or pipette, which is in contact with it) and the collector/ground. After the jet flowed away from the droplet in a nearly straight line, it bent into a complex path and other changes in shape occurred, during which electrical forces stretched and thinned it by very large ratios. After the solvent evaporated birefringent nanofibers were left. The above scenario is characteristic of the experiments conducted by a number of groups with very minor. Templates for manufacturing nanotubes are also electrospun by the same method. The existing reviews of electrospinning mostly deal with the material science aspects of the process and applications of the as-spun [43].

2.3.1 Electrospinning process

Electrospinning basically comprises of three components to fabricate nanofibers: a high voltage supplier, a capillary tube with a pipette or needle of small diameter, and a metal collecting screen. (Figure 2.6) In the electrospinning process a high voltage is used to emerge an electrically charged jet of polymer solution or melt out of the pipette.

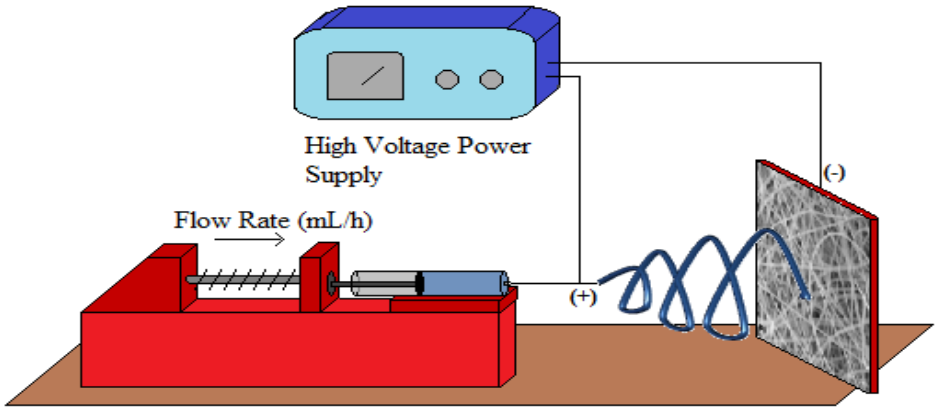

Figure 2.6: Schematic diagram of an electrospinning apparatus.

Before reaching the metal collector on which are covered with aluminium foil, the solution jet evaporates, and is collected as an interconnected web of small fibers [44]. One electrode is placed into the spinning solution/melt and the other attached to the collector. Most of the polymers are dissolved in some solvents before electrospinning, and when it completely dissolves, forms polymer solution. The polymer fluid is then introduced into the capillary tube for electrospinning [45].

In the electrospinning process, a polymer solution held by its surface tension at the end of a capillary tube is subjected to an electric field and an electric charge is induced on the liquid surface due to this electric field. When the electric field applied reaches a critical value, the repulsive electrical forces overcome the surface tension forces. Eventually, a charged jet of the solution is ejected from the tip of the Taylor cone and an unstable and a rapid whipping of the jet occurs in the space between the capillary tip and collector which leads to evaporation of the solvent, leaving a polymer behind [46-48].

2.3.2 Effects of parameters on electrospinning

There are a number of parameters and processing variables that affect the electrospinning process: (i) system parameters such as molecular weight, molecular weight distribution and architecture (branched, linear, etc.) of the polymer, and polymer solution properties (viscosity, conductivity, dielectric constant, and surface tension, charge carried by the spinning jet) and (ii) process parameters such as electric potential, flow rate and concentration, distance between the capillary and

collection screen, ambient parameters (temperature, humidity and air velocity in the chamber) and finally motion of the target screen [40].

2.3.3 Solution parameters

2.3.3.1 Concentration

The concentrations of polymer solution play an important role in the fiber formation during the electrospinning process. Four critical concentrations from low to high should be noted:

- At lower concentrations, polymeric micro (nano)-particles will be obtained. At this time, electrospray occurs instead of electrospinning owing to the low viscosity and high surface tensions of the solution [49].
- At a bit higher concentrations, a mixture of beads and fibers will be obtained [50].
- When the concentration is suitable, smooth nanofibers can be obtained [50]
- If the concentration is very high, not nanoscaled fibers, helix-shaped microribbons will be observed [51].

In general, increasing the concentration of solution, the fiber diameter will increase if the solution concentration is suitable for electrospinning. Additionally, solution viscosity can be also tuned by adjusting the solution concentration.

2.3.3.2 Molecular weight

Molecular weight of the polymer also has an important effect on morphologies of electrospun fiber. In principle, molecular weight reflects the entanglement of polymer chains in solutions, namely the solution viscosity. Keep the concentration fixed, lowering the molecular weight of the polymer trends to form beads rather than smooth fiber. Smooth fiber will be obtained with the increasing molecular weights. Further increasing the molecular weight, micro-ribbon will be obtained [52].

It is also important to note that too high molecular weight favors the formation of micro-ribbon even with the low concentration [53]. Additionally, the authors found that as the molecular weight is very high, some patterned fibers can also be obtained at low concentration. However, it is also important to point out that the molecular weight is not always essential for electrospinning if sufficient intermolecular interactions can be supplied by oligomers.

2.3.3.3 Viscosity

Solution viscosity is the critical key in determining the fiber morphology. It has been proven that continuous and smooth fibers cannot be obtained in very low viscosity, whereas very high viscosity results in the hard ejection of jets from solution, namely there is a requirement of suitable viscosity for electrospinning [54]. Generally, the solution viscosity can be tuned by adjusting the polymer concentration of the solution; thus, different products can be obtained. The viscosity range of a different polymer or oligomer solution at which electrospinning is done is different. It is important to note that viscosity, polymer concentration, and polymeric molecular weight are related to each other. For solution of low viscosity, surface tension is the dominant factor and just beads or beaded fiber formed. If the solution is of suitable viscosity, continuous fibers can be obtained. A number of papers on such interrelationships have been published [55-59].

2.3.3.4 Surface tension

Surface tension, more likely to be a function of solvent compositions of the solution plays a critical role in the electrospinning process and by reducing the surface tension of a nanofiber solution; fibers can be obtained without beads. Different solvents may contribute different surface tensions. Generally, the high surface tension of a solution inhibits the electrospinning process because of instability of the jets and the generation of sprayed droplets [60]. Basically, surface tension determines the upper and lower boundaries of the electrospinning window if all other variables are held stable [61-63].

2.3.3.5 Conductivity/Surface charge density

Solution conductivity is mainly determined by the polymer type, solvent type and the salt. Natural polymers are generally polyelectrolytic in nature, in which the ions increase the charge carrying ability of the polymer jet, subjecting to higher tension under the electric field, resulting in the poor fiber formation in contrast to the synthetic counterpart [64]. Additionally, the electrical conductivity of the solution can be tuned by adding the ionic salts like KH_2PO_4, NaCl etc. [65]. With the aid of ionic salts, nanofibers with small diameter can be obtained. Sometimes high solution conductivity can be also achieved by using organic acid as the solvent.

2.3.4 Processing parameters

Another important parameter that affects the electrospinning process is the distinct external factors which involve the voltage supplied, the flow-rate, type of collector, and distance between the needle tips exerting on the electrospinning jet [66].

2.3.4.1 Applied voltage

The high voltage will induce the necessary charges on the solution and together with the external electric field, will initiate the electrospinning process when the electrostatic force in the solution overcomes the surface tension of the solution. Generally, both high negative or positive voltage of more than 6 kV is able to result in the solution drop at the tip of the needle to distort into the shape of a Taylor Cone during jet initiation [67]. Depending on the feed rate of the solution, a higher voltage may be required so that the Taylor Cone is stable. The columbic repulsive force in the jet will then stretch the viscoelastic solution. If the applied voltage is higher, the greater amount of charges will cause the jet to accelerate faster and more volume of solution will be drawn from the tip of the needle. This may result in a smaller and less stable Taylor Cone [68]. When the drawing of the solution to the collection plate is faster than the supply from the source, the Taylor Cone may recede into the needle [69]. Applied voltage has also effects on the morphology and the resultant fibers. Increase in the applied voltage results with a decrease in the fiber diameter. High voltage causes higher bead formation, but increased jet stretching leads to fewer amounts of beads [70]. Because of the weaker electrostatic force, flight time may become longer at lower voltage. Longer flight time lets the jet to elongate and stretch stronger and longer resulting with reduced fiber diameter. Wang et al. measured both jet diameter and fiber diameter and investigated the effect of voltage difference [71]. They found out that not only jet diameter but also fiber diameter decreased slightly. Furthermore, better chain orientation within electrospun fibers was observed by an increase in the applied voltage. A proportionality relation between applied voltage and fiber diameter was reached in a study [72].

2.3.4.2 Flow rate

The flow rate of the polymer from the syringe is a significant process parameter since it influences the jet velocity and the material transfer rate. A lower feed rate is more desirable as the solvent will get enough time for evaporation [73]. There should

always be a minimum flow rate of the spinning solution. It has been observed that the fiber diameter and the pore diameter increases with an increase in the polymer flow rate in the case of polystyrene (PS) fibers and by changing the flow rate, the morphological structure can be slightly changed. Some studies have systematically researched the relationship between solution feed or flow rate on fiber morphology and size [74].

If the flow rate is at the same rate which the solution is carried away by the electrospinning jet, there must be a corresponding increased in charges connected with the flow rate is increased. Thus, there is a corresponding increase in the stretching of the solution which counters the increased diameter because of increased volume. Due to the greater volume of solution drawn from the needle tip, the jet will takes a longer time to dry. Therfore, the solvents in the deposited fibers could not have enough time to evaporate in the given same flight time. The residual solvents may cause the fibers to fuse together where they make contact forming webs. As a result, a lower flow rate is more desirable as the solvent will have more time for evaporation [71].

2.3.4.3 Distance

The distance (the distance from the terminus of the capillary tip to the surface of the collector) defines the strength of the electric field as well as the time available for evaporation of the solvent before the nanofibers reach the collector surface. Increasing the distance, assuming other parameters constant, usually reduces fiber diameters [75]. Reducing the distance does not affect size and shape of the fibers, but, inhomogeneously distributed beads can be formed [69]. These beads can be due to increase in the electric field strength. If the distance between the tip and the collector is longer, solution jet finds more time for the evaporation of the solvent and jet can be stretched sufficiently before it lands to the collecting media. Increasing the working distance enhances the density of the fibers whereas decreasing the number of beads [76]. Jet diameter dependence on the working distance is studied [77].

2.3.4.4 Effect of collector

In the electrospinning process, usually conductive material is used to cover collecting media. Aluminium foil is one of the most common conductive materials that are used for collection of fibers onto it.

One important aspect of the electrospinning process is the type of collector used. In this process, a collector serves as a conductive substrate where the nanofibers are collected. Generally, aluminium foil is used as a collector but due to difficulty in transferring of collected fibers and with the need for aligned fibers for various applications, other collectors such as, conductive paper, conductive cloth, wire mesh, pin, parallel or grided bar, rotating rod, rotating wheel, liquid non solvent such as methanol coagulation bath and others are also common types of collectors nowadays. With less conductive area, there was generation of beaded fibers because of the less surface area. In another study they compared wire screen with aluminium foil and wire screen without aluminium foil in the same conductive area and found that pure wire screen is a better collector for fiber collection because with the use of wire screen the transfer of fibers to other substrates became easy. The fiber alignment is determined by the type of the target/collector and its rotation speed [78].

2.4 Characterizations

2.4.1 Attenuated total reflection fourier transform infrared spectroscopy (FTIR-ATR)

FTIR is a fundamental tool that is used to probe substances to determine the nature of their molecular bonds.

FTIR has commonly been used for the identification of functional groups among organic molecules. It can often easily distinguish between a variety of molecular bonds involving carbon, hydrogen, nitrogen, oxygen, phosphorus, sulfur, and halogens. Traditionally, FTIR is used with a transmission cell or a KBr pellet. However, in the surface science community, infrared spectroscopy is used in a different manner.

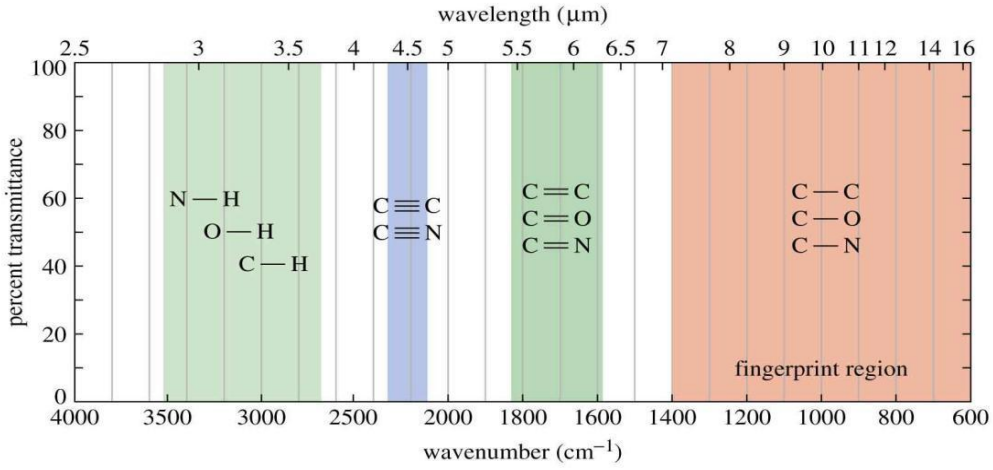

Figure 2.7: Infrared spectrum bands for general subtitutions.

Attenuated Total Reflection (ATR) is an accessory of transmission IR spectrometers that significantly enhances surface sensitivity. As the name implies, ATR refers to a particular type of reflection geometry. In contrast to transmission FTIR, in which the infrared beam travels in a straight path through a sample, in ATR, the infrared beam is reflected internally through a crystal. The beam is oriented to bounce within the crystal at an angle that ensures total internal reflection. Just above each point of reflection exists an evanescent wave that can probe substances within about a micrometer of the crystal surface.

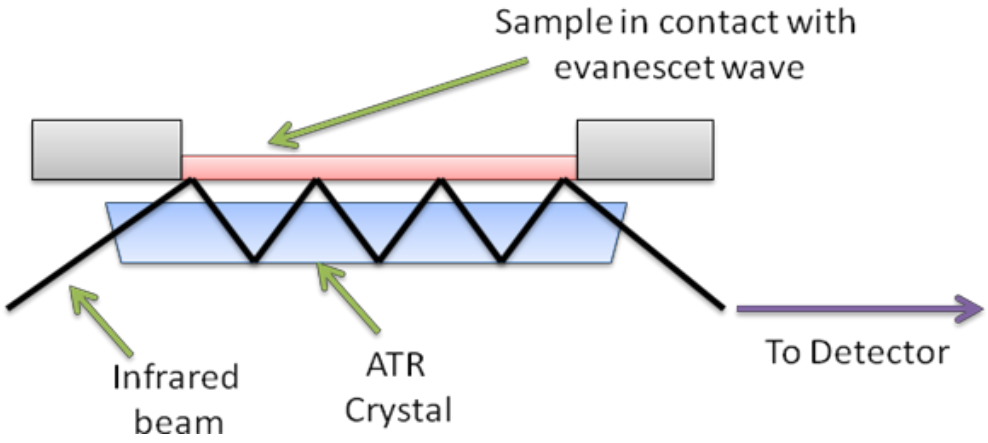

Figure 2.8: A multiple reflection ATR system.

2.4.2 Scanning electron microscope

Scanning electron microscopy (SEM) is one of the most widely used techniques in nanomaterials characterization. This method usually is applied to get information about the grain size, surface roughness, porosity, particle size distributions, material homogeneity, and intermetallic distribution and diffusion.

The electron beam, which typically has an energy ranging from a few hundred eV to 50 keV, is focused by one or two condenser lenses into a beam with a very fine focal spot sized 1 nm to 5 nm. The beam passes through pairs of scanning coils in the objective lens, which deflect the beam in a raster fashion over a rectangular area of the sample surface. Through these scattering events, the primary electron beam effectively spreads and fills to teardrop-shaped volume, known as the interaction volume, extending from less than 100 nm to around 5µm into the surface.

Interactions in this region lead to the subsequent emission of electrons which are then detected to produce an image. X-rays, which are also produced by the interaction of

electrons with the sample, may also be detected in an SEM equipped for energy-dispersive X-ray spectroscopy or wavelength dispersive X-ray spectroscopy.

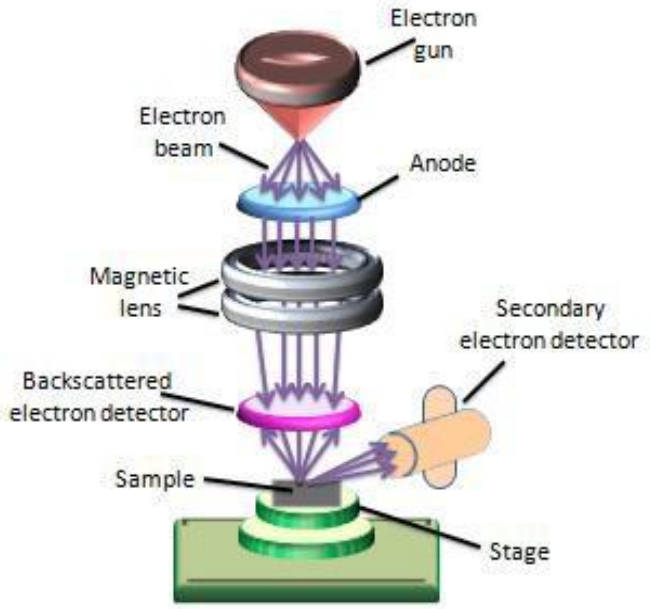

Figure 2.9: Schematic diagram of scanning electron microscopy.

2.4.3 Atomic force microscopy (AFM)

AFM is one of the most powerful tools for determining the surface topography of native biomolecules at subnanometer resolution. The technique involves imaging a sample through the use of a probe, or tip, with a radius of several nm. The tip is held several nanometers above the surface using a feedback mechanism that measures surface–tip interactions on the scale of nanoNewtons. Variations in tip height are recorded while the tip is scanned repeatedly across the sample, producing a topographic image of the surface. Atomic force microscope is capable to produce images in different modes including tapping, magnetic force, electrical force, and pulsed force.

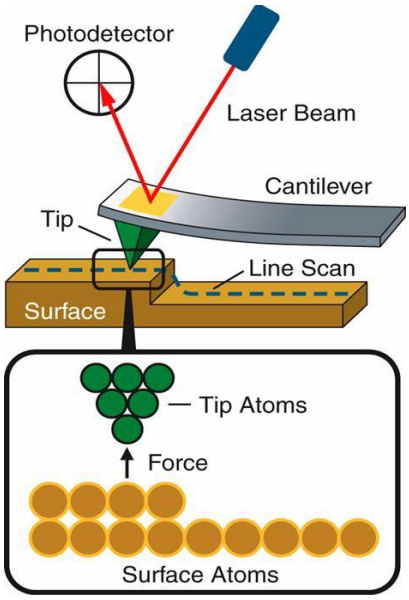

Figure 2.10: Schematic diagram of atomic force microscope.

AFM works by bringing a cantilever tip in contact with the surface to be imaged. An ionic repulsive force from the surface applied to the tip bends the cantilever upwards. The amount of bending, measured by a laser spot reflected on to a split photo detector, can be used to calculate the force. By keeping the force constant while scanning the tip across the surface, the vertical movement of the tip follows the surface profile and is recorded as the surface topography by the AFM.

2.4.4 Electrochemical Impedance Spectroscopy (EIS)

Electrochemical Impedance Spectroscopy (EIS) is a powerful tool to investigate chemical and physical processes at liquid/solid interfaces. EIS is becoming increasingly popular for a number of applications such as; characterisation of batteries, fuel cells, organic coatings, ceramics, semiconductors, sensors, and conducting polymers as well as for corrosion studies [79-80].

In dc theory, the applied potential E (Volt) is related to the current I (Ampere) by

Ohm‟s law defining the resistance R (Ohm):

$$E=I.R \qquad \textbf{(2.1)}$$

In AC theory, in the analogous equation of R the impedance Z is defined:

$$E=I.Z \qquad \textbf{(2.2)}$$

Figure 2.11 shows the relationship between current and voltage in impedance measurements.

In an EIS measurement, a small excitation signal is applied and electrochemical impedance response is measured. In a linear system, the current response to a sinusoidal potential will be a sinusoid at the same frequency but shifted in phase.

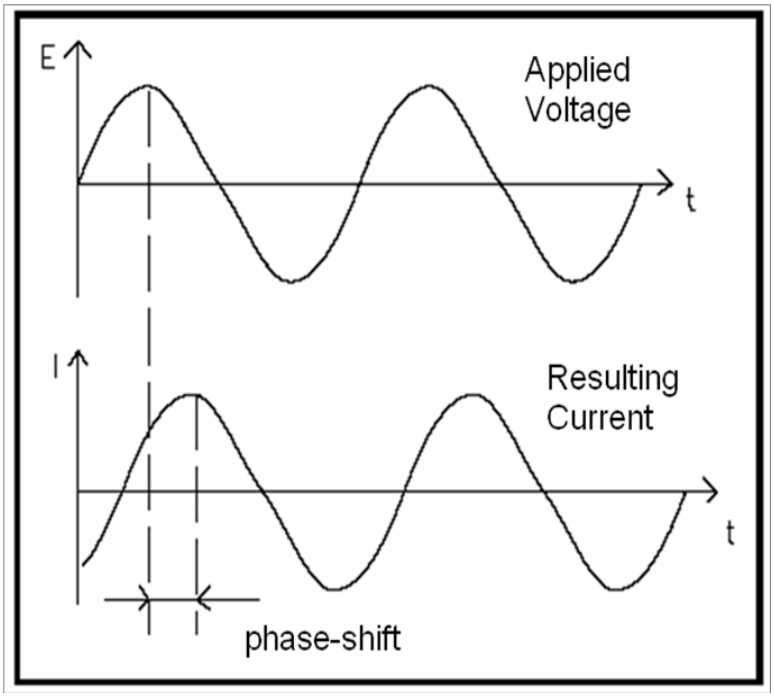

Figure 2.11: Relationship between current and voltage in impedance measurements.

The excitation signal that is applied to the cell has the form:

$$E(t) = Eo \sin(\omega t) \quad \textbf{(2.3)}$$

E(t) is the potential at time tr Eo is the amplitude of the signal, and ω is the radial frequency. The relationship between radial frequency ω (expressed in radians/second) and frequency f (expressed in hertz) is:

$$\omega = 2\,\pi f \quad \textbf{(2.4)}$$

For the linear system, the resulting current is given by the equation:

$$I_0 = I_t \sin(\omega t + \varphi) \quad \textbf{(2.5)}$$

Here φ is the phase difference between the voltage and the current.

The perturbation potential and the current respond can be written as complex function:

$$E_0 = E_e \exp(i\omega t) \quad \textbf{(2.6)}$$

$$I_0 = I_e \exp(i\omega t) - \emptyset \quad \textbf{(2.7)}$$

The impedance is defined as the ratio between potential and current:

$$Z = (E/I)\, Z_0 \exp(i\varphi) = Z_0\,(\cos\emptyset + i\sin\emptyset) \quad \textbf{(2.8)}$$

Impedance data is typically represented in two types of plots: the Nyquist Plot and the Bode Plots.

The Nyquist Plot, where the X-axis represents the real part and the Y-axis represents the imaginary part of the complex number. In the case of plotting impedance data, the positive Y-axis conventionally represents the negative imaginary portion of the impedance and there is a complex impedance point for every frequency at which the impedance was measured, creating a plot with impedance features.

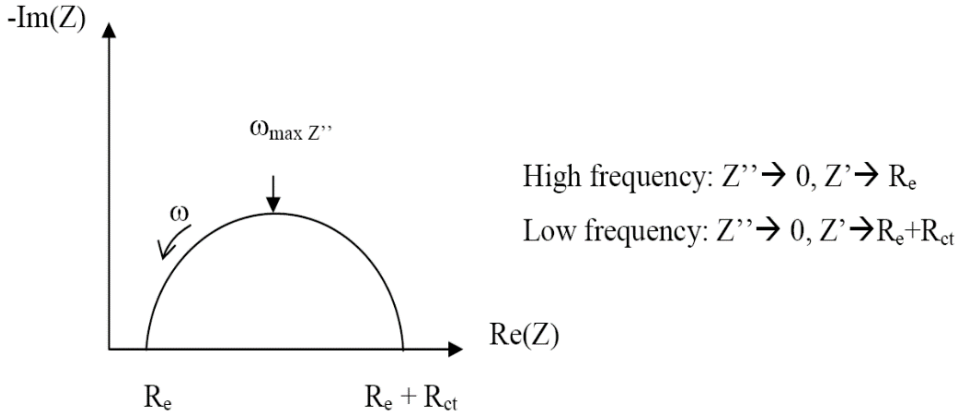

Figure 2.12: Nyquist plot of the impedance of a simple electrode reaction.

The Nyquist plot of the impedance of the simple electrode reaction is a semicircle (Figure 2.11). The intercept of the plot with the axis (high frequency) is Re (electrolyte resistance or solution resistance). The other intercept at low frequency is the sum of Re and Rct. The Nyquist plot has some advantages and disadvantages.

Advantages:

- A simple representation of the Re
- The shape of plot does not change when the ohmic resistance is changed.
- A simple representation of the charge transfer resistance as diameter of the semi circle.

Disadvantages:

- Indirect representation on frequency

The Bode Plot consists of two graphs. Impedance Z and phase angle φ are presented as a function of frequency (in logarithmic form). The Re and Re +Rct value can be taken from the value of |Z| for ω→∞ and ω→0. At intermediate frequencies, the plot of logZ should be a straight line with slope –1. Extrapolating this line to ω →1 gives the value of 1/ Cdl.

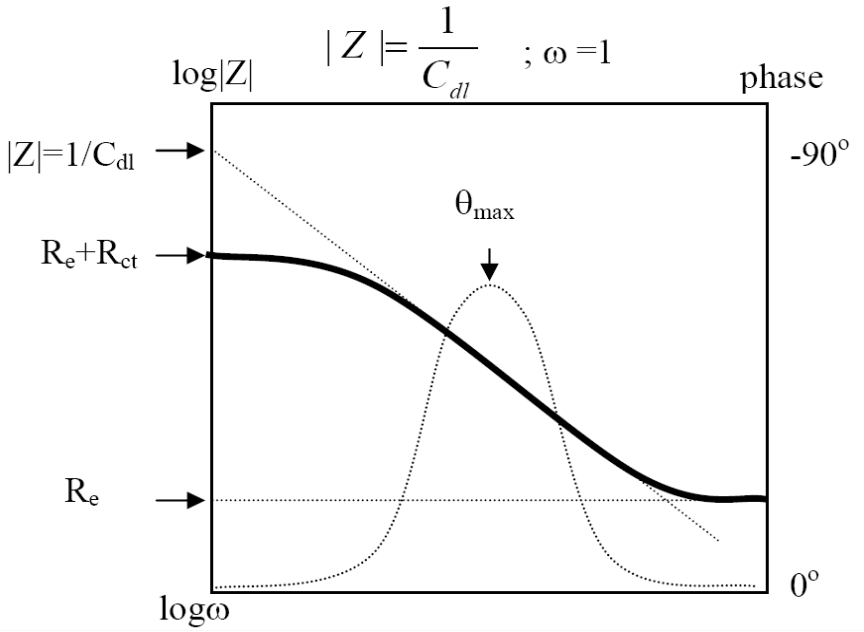

Figure 2.13: Bode plot for a simple electrochemical system (impedance - solid line, phase angle - dotted line).

The phase angle is nearly zero for $\omega \to \infty$ and $\omega \to 1$. It has the maximum for medium frequencies. The Bode plot provides a clear description of the frequency-dependence of the electrochemical parameters.

3. EXPERIMENTAL PART

3.1 Materials

CTAB, CPC and PVP (Mw= 1.300.000 $g.mol^{-1}$) obtained from Sigma Aldrich, Germany, were used without further purification. Ethanol (EtOH; Merck, Germany) and phosphate buffer solution (PBS; Merck, Germany) were chosen as solvents. All the bacteria (Klebsiella pneumonia ATCC 4352, Staphylococcus aureus ATCC 6538 and Escherichia coli ATCC 10536) obtained from ATCC, and Luria Bertani Broth and Luria Bertani agar were obtained from Sigma Life Sciences (Germany).

3.2 Analysis and Characterization Techniques

PVP, PVP/CTAB and PVP/CPC nanofibers were analyzed and characterized using Fourier Transform Infrared Spectroscopy (FTIR), Scanning Electron Microscopy, (SEM), Atomic Force Microscopy (AFM) and electrochemical measurements were performed by Electrochemical Impedance Spectroscopy (EIS).

FTIR spectra of the samples were recorded on Perkin Elmer Spectrum One (FTIR-reflectance, Universal ATR with diamond and ZnSe, USA) spectrophotometer. The SEM images were obtained using Zeiss EVO MA10 microscope with standard tungsten filament. AFM images were obtained with Nanosurf Easy Scan 2™. In all AFM analyses, the non-contact mode was employed by using ACLA-20 model, Al-coated high resonance frequency silicon tips (145 kHz) with 7 µm thicknesses, 43 µm mean width, 225 µm length and 48 N/m force constant. High resolution images (1024 × 1024 pixels) and the raw data were collected by the Easy Scan 2™ (version 1.5.0.0.) software (Japan).

Fibers were used as ITO-PET coated working electrode, Pt wire was used as the counter electrode, and a silver (Ag) wire as the pseudo-reference electrode was used for all electrochemical characterizations in Phosphate Buffer Solution (PBS) system by using a Parstat 2263 potentiostat. All fibers were doped before analysis at 1.5 V for 10 minutes. The electrochemical activity of the fibers was evaluated from data obtained by EIS in the frequency of 10 mHz to 10 kHz. Equivalent circuit was used to fit the experimental data, with the help of the ZsimpWin v3.10 software. The bulk

conductivities were calculated from the bulk resistance value obtained from the complex impedance diagram.

3.3 Preparation of PVP/CTAB and PVP/CPC Fibers via Electrospinning

The CTAB (or CPC) containing nanofibers were prepared by electrospinning (Figure 2.6) from a solution of PVP prepared with 10.0 g dissolved in 100mL EtOH as solvent and defined as 10.0 wt/vol% PVP. The CTAB (or CPC) contained solutions were also prepared with PVP/CTAB (PVP/CPC) in weight percents' based to EtOH solvent volume at different ratios varying from 10.0/0.50 % to 10.0/5.0 % were prepared by mixing the solution with a magnetic stirrer for 24 h at room temperature and is given in Table 3.1. Blended solutions were poured into a 2 mL syringe and delivered at a constant flow rate of 1.0 mL/h (New era, NE-300) to a needle with a diameter of 0.7 mm and a blunt tip connected to a high voltage power supply (Gamma High Voltage Research). At 15 cm distance and 10 kV applied voltage, the solvent evaporated and charged polymers were deposited on the aluminum foil collector in the form of nanofibers for a period of 30 minutes. The nanofibers used for antibacterial efficacy determination were deposited onto the collector for a period of 4 hours to achieve an areal density of 0.4 g/cm^2. The obtained nanofibers were vacuum-dried until the residual solvent evaporated.

Table 3.1: Electrospinning parameters for various composites

Electrospinning Parameters	
Solution concentration	% 10
Applied voltage	10 kV
Tip-to-collector distance	15 cm
Feed rate	1 ml/h

3.4 Electrospinning Process Setup

The metal collector was covered with an aluminum foil. The process was conducted in a plexiglass box for experimenter's safety. All experiments were carried out under atmospheric pressure and at room temperature. The positive electrode wire was hooked at the metal part of the needle and negative part of the electrode was attached to the metal collector. 3 to 4 hours of operation time was sufficient for the deposition of fibers on aluminum foil to have antibacterial analysis and 1 hour of operation time

onto ITO-PET was sufficient to perform electrochemical analysis. A horizontal setup was chosen for electrospinning process.

3.5 Determination of Antibacterial Activity

Antibacterial activity of textile samples has been determined according to a modified version of standards of ISO 20743:2007 entitled as "Textiles-Determination of antibacterial activity of antibacterial finished products". In the content of this international standard, plate count methodology as a quantitative test method has been applied to determine the antibacterial activity of the samples. Despite the fact that standard proposes two bacteria, one from gram negative (*Klebsiella pneumonia* ATCC 4352) and the other from gram positive (*Staphylococcus aureus* ATCC 6538) to test antibacterial activity, a third bacteria (*Escherichia coli* ATCC 10536) has also been used to test the samples. All the bacteria were obtained from ATCC, and Luria Bertani Broth and Luria Bertani agar were obtained from Sigma Life Sciences (Germany). Bacteria were grown on enumeration agar, pH = 7.2 ± 0.2, containing dehydrated yeast extract, casein tryptone, glucose, and agar. Afterwards, one colony was placed in 20 ml of nutrition broth, pH = 6.9 ± 0.2, composed of beef extract, peptone, and water, for 18-24 hours at 37°C. Inoculums from the previous step (0.4 ml) were placed in 20 ml of nutrition broth and incubated for additional 3 ± 1 hour in order to obtain the concentration of bacteria of 10^7 Colony Forming Units/ml. Concentration of 1×10^5 CFU/ml to 3×10^5 CFU/ml was adjusted by spectrophotometer (BioRad, Hercules, CA, USA).

Four different nanofibrous webs with different CTAB ratios of 0.50 % (wt/vol) - 5.0 % (wt/vol) in 10.0 wt/vol% of PVP and the PVP web alone as control were cut to obtain 0.2g±0.05g of paired test samples (Table 3.1). Thus, a total of ten test and control samples were obtained for each bacterium. 1 ml of the inoculum was added into a test tube containing 9.0 ml ± 0.1 ml of the nutrient broth and shaken well for a homogenous distribution. Serial dilutions were prepared and 1 ml of each dilution was pipetted into two petri dishes containing 15 ml of LBA for each sample, then all the dishes were incubated at 37 °C ± 2 °C for 24 h to 48 h.

After incubation, the number of colonies on the petri dishes of dilution series was counted and the bacteria concentration in the solution was calculated according to the following formula:

$$C_B = Z \cdot R \quad \textbf{(3.1)}$$

where C_B is the bacteria concentration in Colony Forming Units per milliliter (CFU/ml); Z is the average value in Colony Forming Units (CFU) in the two petri dishes; R is the dilution rate.

4. RESULTS AND DISCUSSIONS OF PVP/CTAB

4.1 Morphological Analysis of PVP/CTAB

4.1.1 Scanning electron microscopy

PVP/CTAB ratios (%wt/vol) of different nanofibrous web samples and their corresponding average fiber diameters are presented in Table 4.1. To determine the average fiber diameters, fifty measurements were taken from each sample and then the average values were calculated. SEM micrographs of five different samples containing different PVP/CTAB ratios can be seen in Figure 4.1. As seen from Figure 4.1a, the PVP nanofibers have a smooth surface with a diameter range of 555±86 nm. The micrographs of PVP/CTAB blends (Figure 4.1 b-e) demonstrate the presence of CTAB salt in the form of crystalline particles clearly visible on the fibers. The introduction of CTAB salt into the nanofibers affected the fiber morphology by a decrease in the average fiber diameter of PVP/CTAB samples ranging from ~500 nm to ~200 nm compared to that of the pristine PVP samples without salt (Figure 4.2).

Table 4.1: PVP and CTAB ratios (%wt/v) of five different nanofibrous web samples

Sample No	PVP (%wt/v)	CTAB (%wt/v)	Fiber diameter (nm)
S1 (control)	10.0	0.00	555 ±86
S2	10.0	0.5	490 ±12
S3	10.0	1.0	323 ±19
S4	10.0	2.5	252 ±12
S5	10.0	5.0	213 ±93

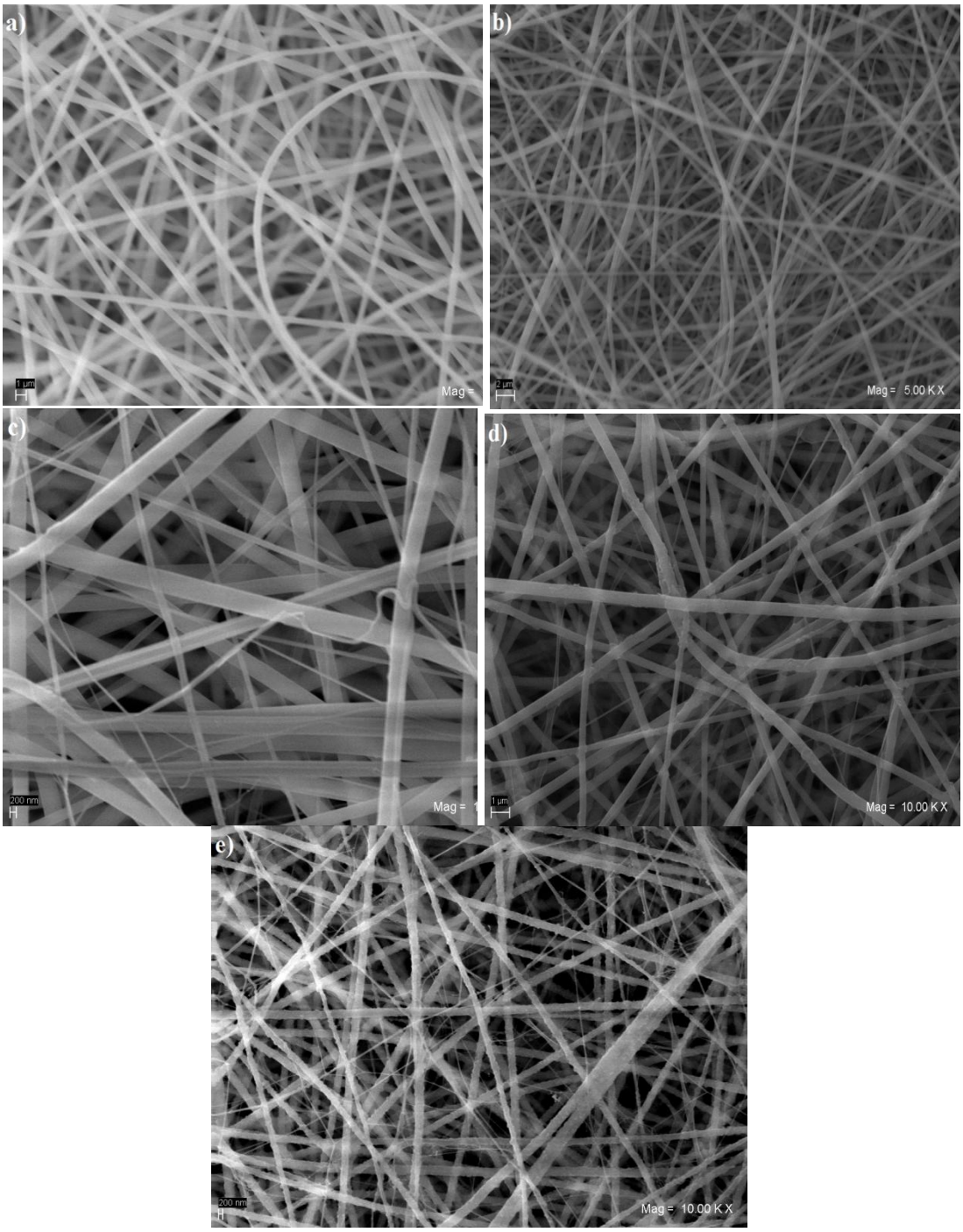

Figure 4.1: SEM of electrospun of samples a) S1, b)S2, c) S3, d) S4 and e) S5 at a magnification of 5000x-15000x using constant electrospinning parameters of 10 kV voltage, the needle collector distance of 10 cm and a flow rate of 1.0 mL/h.

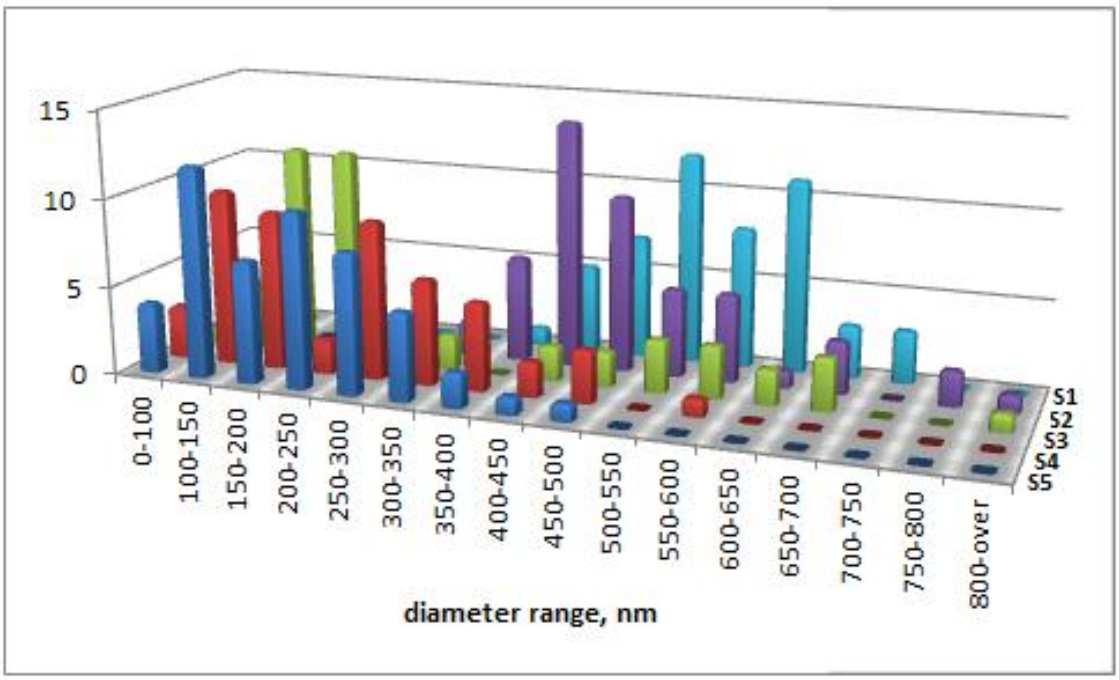

Figure 4.2: Fiber diameter distribution for the samples S1 through S5.

4.1.2 Atomic Force Microscopy

The AFM micrographs of the control sample S1 and sample S5 having the highest CTAB content with 5.0 % (wt/vol) are shown in Figure 4.3. As seen from Figure 4a and b, the pristine PVP nanofibers have a smooth surface and a homogenously dispersed structure with a surface roughness of 139.76 nm, calculated with Nanosurf software. Sample S5 demonstrates the presence of CTAB salt crystalline particles with a roughening effect on the fibers resulting in an increase in surface roughness by 180.96 nm (Figure 4.3 c and d).

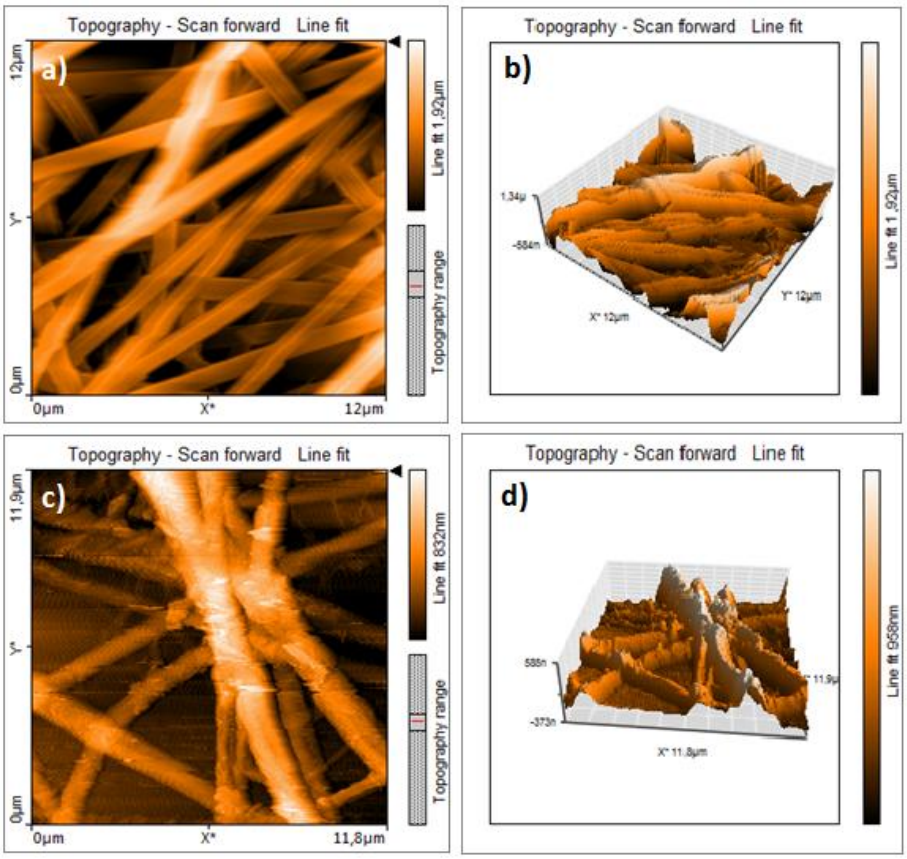

Figure 4.3: AFM micrographs of samples S1 (a, b) and S5 (c, d).

4.2 FTIR-ATR Analysis of PVP/CTAB

As can be seen from the FTIR absorbance spectrum in Figure 4.4, PVP and CTAB possessed common peaks. The bands with peak locations at 2825 and 2875 cm^{-1} existed due to the C-H stretching of the ring CH groups on the side chains. In addition, a series of bands at 1425 cm^{-1} were attributed to the C-C bond (stretching) of the aromatic rings. Bands with peak locations at 750 cm^{-1} (out-of-plane) and 690 cm^{-1} (in-plane) due to the H–C bonds were visible for both PVP and CTAB. The sharp peak at 2915 cm^{-1} corresponding to the C-H stretching vibration of the CH_2 and CH groups on the main chain are characteristic for CTAB. Also The characteristic peaks for PVP existed at 1655cm^{-1} corresponding to the C=O stretching of the aromatic ring, and at 1285 cm^{-1} and 1500 cm^{-1} due to the C-N bonds and C-H bending, respectively. The absorbance (A) was found to increase with the increase in CTAB content as seen in Figure 4.4.

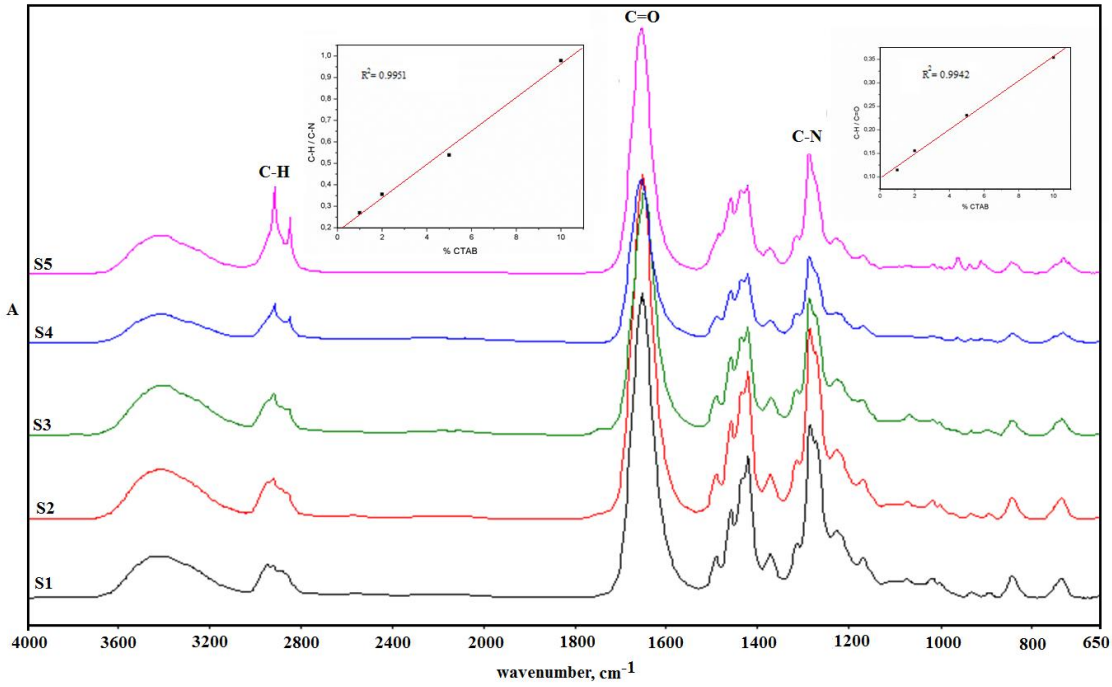

Figure 4.4: FT-IR absorbance spectrum of samples a) S1 ; b) S2 ; c) S3 ; d) S4 and e) S5. Inset: C-H/C=O and C-H/C-N ratios.

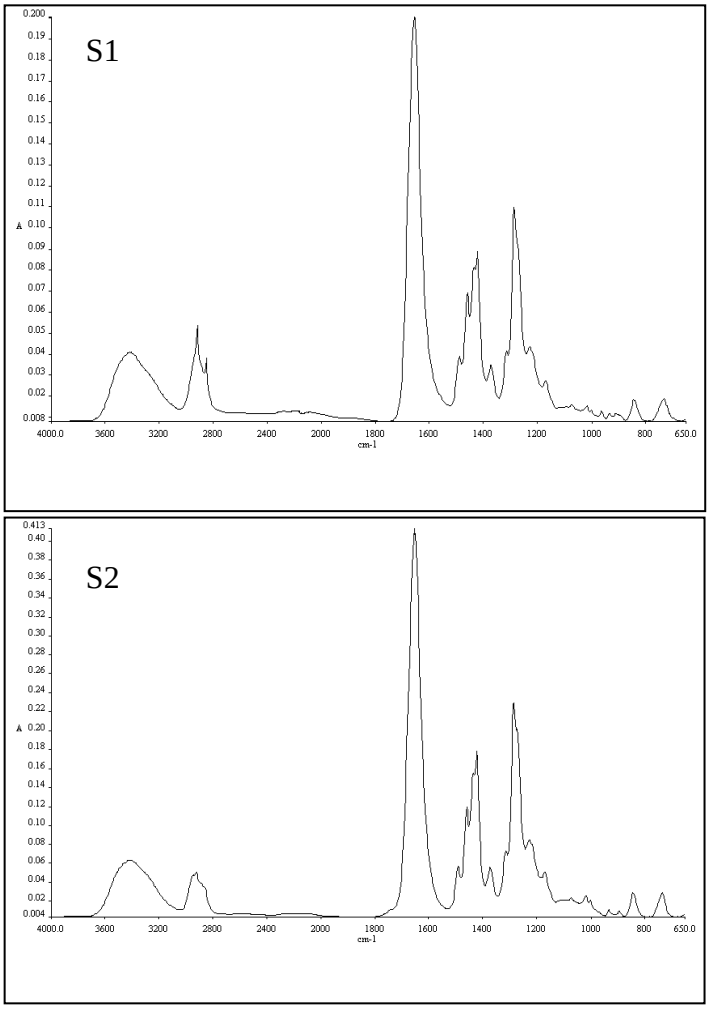

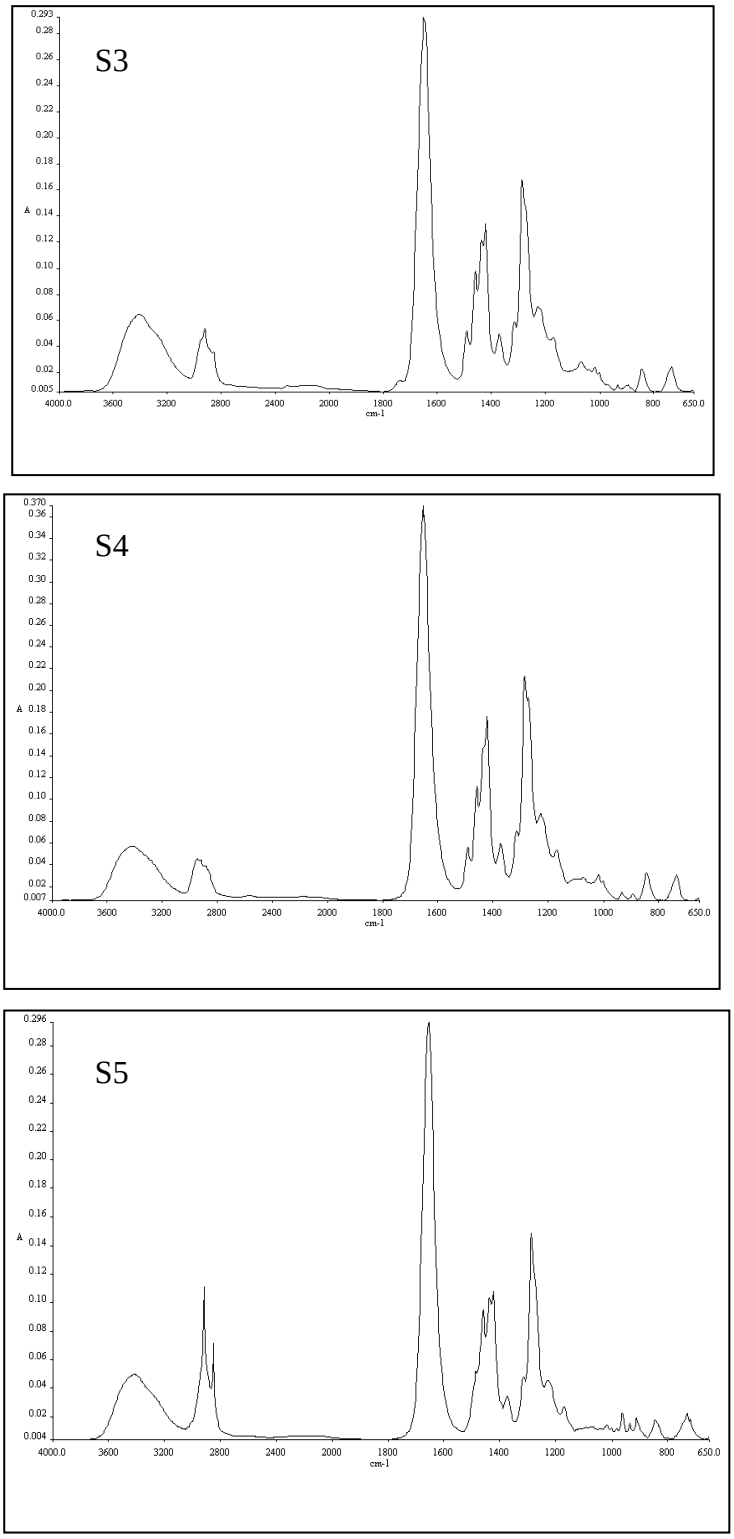

Figure 4.5: FTIR absorbance spectrum of S1-S5, separately

As seen from Figure 4.6, the peak observed at 1650 cm^{-1}, corresponding to the cyclic PVP carbonyl, was ruptured due to the thermal process resulting in a ring opening reaction as defined in Figure 4.7. The peak at 1720 cm^{-1}, corresponding to the alkyl

carbonyl group, resulted from the formation of the crosslinked PVP structure which is insoluble in organic solvents, while a slight solubility in aqueous media was seen for polyvinylpolypyrrolidone (PVPP) samples. Although crosslinking of PVP has been mentioned in different researches [81-83], no detailed description on its mechanism has been reported. The possible crosslinking mechanism for PVP is described in Figure 4.7.

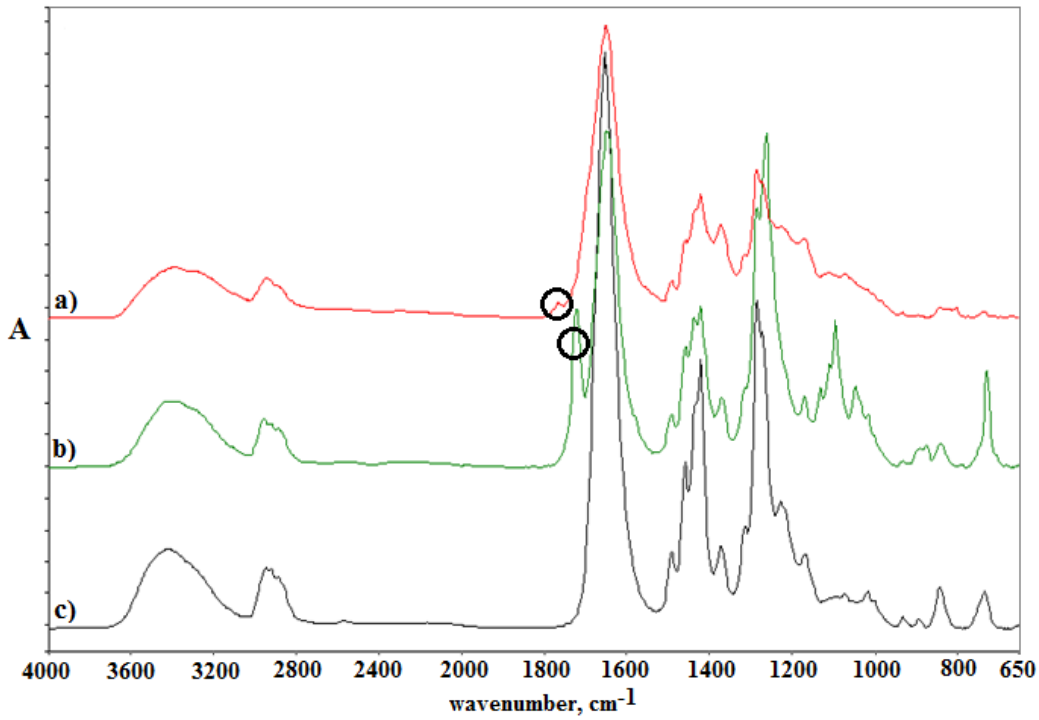

Figure 4.6: FT-IR absorbance spectrums of (a) thermally, (b) UV cured PVPP and (c) PVP.

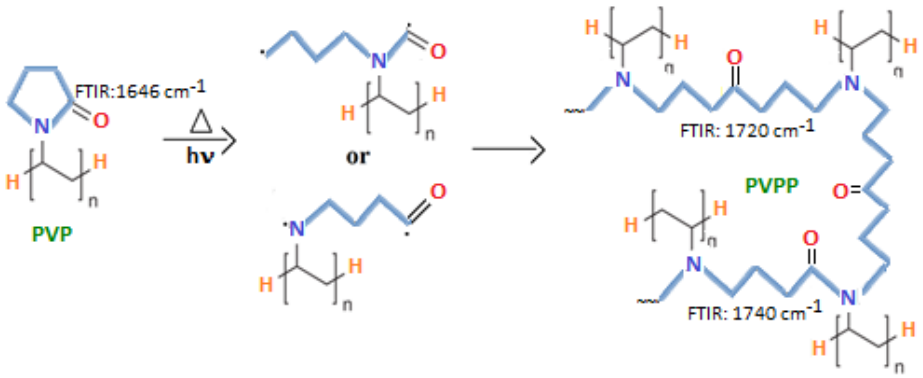

Figure 4.7: Schematic representation of ring opening and crosslinking process.

4.3 UV Spectrophotometric Analysis of PVP/CTAB

Figure 4.8 shows the UV spectrum of thermally cured, sample S5, having a PVPP/CTAB ratio of 10.0/5.0 % (wt/vol). The sample released a high CTAB concentration in PBS solution over time. As seen from Figure 4.8, a peak at 275 nm was observed in PBS after 24 hours [84]. The increased dissolution of the bromide ions into the solution after 2 days was the evidence of the solubility of sample S5 in PBS. The peak reached to a maximum in absorbance at day 2 and stabilized during 7 days period described at arrow end point in Figure 4.8. The maximum wave reached within a week period was still lower than the total bromide concentration existed in CTAB salt itself, which was marked with a star in Figure 4.8.

On the other hand, the non-crosslinked PVP/CTAB nanofibrous sample reached to a maximum peak in the first hour, because of the full dissolution of PVP releasing CTAB to the PBS solution. To get rid of confusion the curve of sample the no thermaly treated S1 sample has a similar absorbance to CTAB salt alone sample (*) in PBS and was not inserted to the graphic.

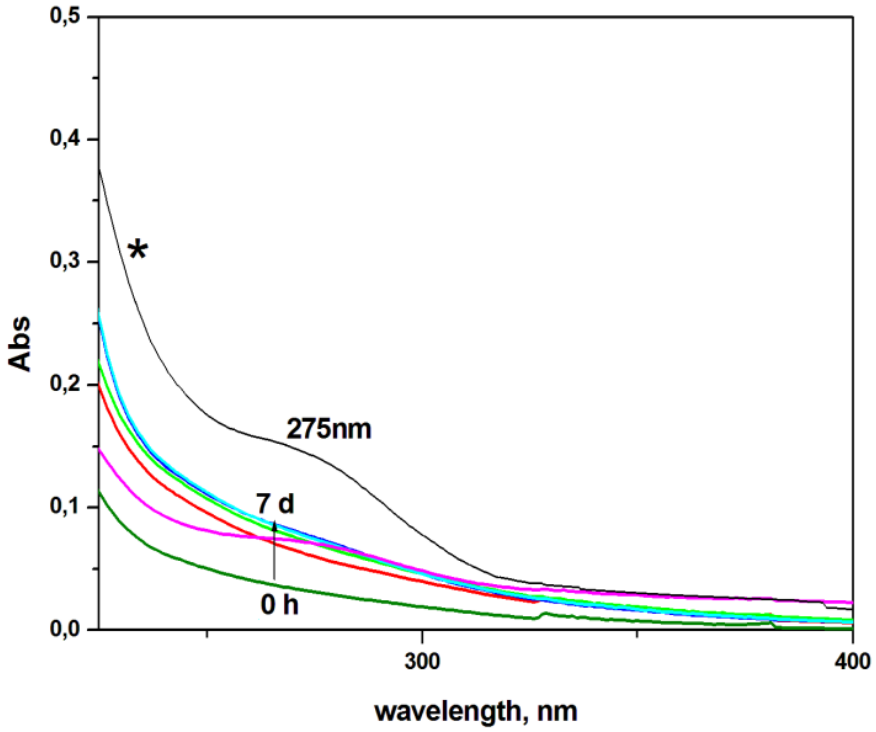

Figure 4.8: Absorption spectra of solutions containing PVPP/CTAB and CTAB salt alone (*) at same weight content recorded immediately after immersion and after 1 week.

4.4 Antibacterial Activity Analysis of PVP/CTAB

Klebsiella pneumonia ATCC 4352 (gram negative), *Staphylococcus aureus* ATCC 6538 (gram positive) bacteria as mentioned in the standard and also *Escherichia coli* ATCC 10536 (gram negative) bacteria were used to evaluate the antibacterial activity of the nanofibrous samples according to a modified version of standards of ISO 20743.

After incubation, the number of colonies on the petri dishes of dilution series (Figure 4.9) was counted as 30 CFU (colony forming units) to 300 CFU, which were converted into logarithmic scale (Table 4.2). The antibacterial activity of the tested samples (S1 to S5) against three bacteria are given in Table 4.2; where the numbers in logarithmic scale show the mean values obtained from duplicate samples. S1 sample, which did not contain any CTAB and used as negative control has shown no antibacterial effectiveness. Those –containing increased concentrations of CTAB from 0.5% (wt/vol) in sample 2 (S2) to 5% (wt/vol) in sample 5 (S5) have shown an effective antibacterial activity, particularly the efficacy was highest in samples S4 and S5 (Figure 4.9). *Escherichia coli* ATCC 10536 was more resistant to the CTAB concentration until the S4 sample compared to the other two bacteria, namely, *Klebsiella pneumonia* ATCC 4352 and *Staphylococcus aureus* ATCC 6538; thus for all three bacteria, an effective antibacterial activity has been realized for a minimum CTAB ratio of 2.5% (wt/vol).

Table 4.2: Bacterial activity of control and CTAB containing samples in logarithmic scale.

Samples	*E. Coli-*	*K. pneumonia -*	*S. aureus+*
S1	0	0	0
S2	0	-1	-1
S3	-3	-5	-5
S4	-5	-5	-5
S5	-5	-5	-5

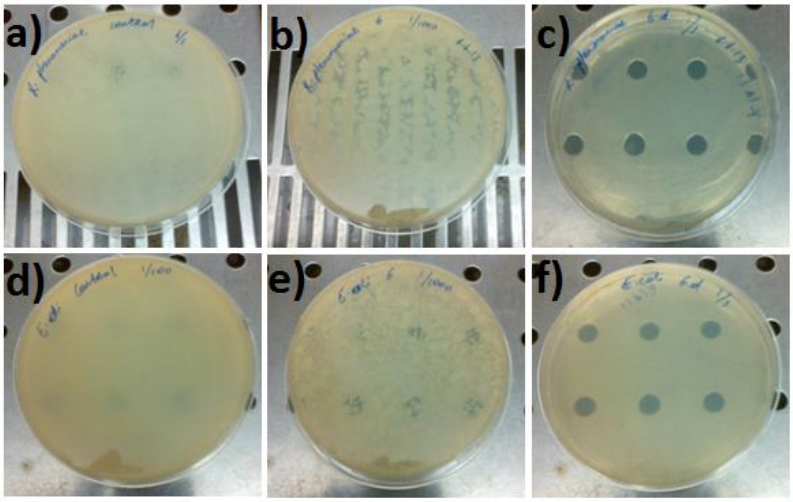

Figure 4.9: Pictures on control sample (a, d), sample S1 (b, e) and sample S5 (c, f) for *K. pneumonia* (ATCC 4352) and *E.coli* (ATCC 10536) bacteria, reciprocally.

4.5 Electrochemical Impedance Spectroscopy (EIS) Analysis of PVP/CTAB

The electrochemical activity of the Br ions, incorporated to the nanofibrous samples by the CTAB presence, was determined using electrochemical impedance spectroscopy (EIS) method. PVP and CTAB/PVP nanofiber coated ITO electrodes were used for EIS measurements and the results are shown in Figures 4.10-4.12. The electrodes were thermally cured for 24 hours at 150^{o}C to obtain a non-soluble crosslinked PVPP. EIS, being known as a nondestructive technique, conducted at a 10 mV frequency band according to open circuit potential where the fiber surface was not harmed during the analysis. An ITO-PET electrode surface was used to determine the electroactivity of CTAB, PVP and the solvent. The measurements were done in a phosphate buffer solution (PBS), where CTAB dissolves over time as was shown in Figure 4.8. As seen from the Nyquist diagram in Figure 4.10, the fiber electrodes consisted of a double semi-circular structure. The first semicircle was related to the double layer capacitance (C_{dl}) and the charge transfer resistance (R_{ct}). The second semicircle was related to the electrode behavior, depending on the CTAB content and the preparative conditions of the fiber. Specific capacitance values were calculated via the formula $C_{sp} = 1 / 2\pi fZ''$ where C_{sp} shows the specific capacitance, f the frequency in Hz and Z'' the imaginary value at that point.

At 10 mHz frequency, samples S3, S4 and S5 showed the capacitance values of 1.06 $mF.cm^{-2}$, 1.01 $mF.cm^{-2}$ and 1.17 $mF.cm^{-2}$, respectively. Bode magnitude plot is used to determine the double-layer capacitance C_{dl} by extrapolating a line to log Z axis at $\omega = 1$ Hz yielding the value of C_{dl} by the relationship: $|Z| = 1 / C_{dl}$.

The double layer constant phase element Q_{dl} was found to increase with CTAB content, being 12.06 $\mu S.s^{-n}.cm^{-2}$, 20.82 $\mu S.s^{-n}.cm^{-2}$ and 21.81 $\mu S.s^{-n}.cm^{-2}$ for the samples S3, S4 and S5, respectively, while the charge transfer resistance decreased stepwise from 7545 $\Omega.cm^{-2}$ to 523 $\Omega.cm^{-2}$. On the other hand, the Bode phase plot phase angle approaches to a plateau in the frequency region of 100 mHz–10 Hz having a value varying between 60-80° with the CTAB content.

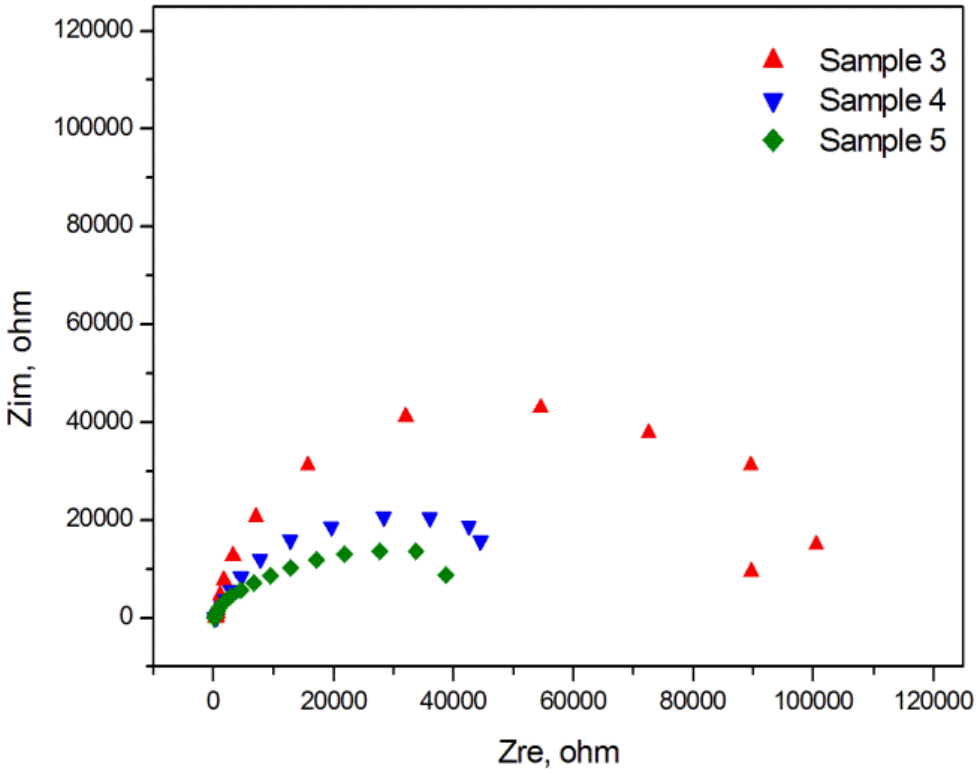

Figure 4.10: Nyquist plot of samples S3, S4 and S5 in PBS.

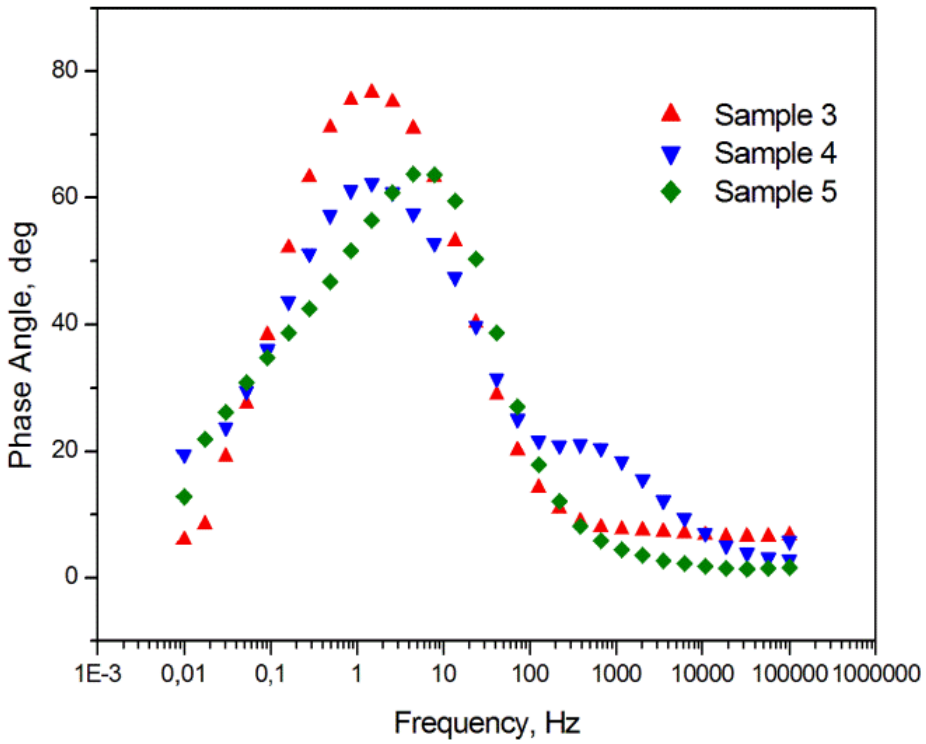

Figure 4.11: Bode Phase plot of samples S3 , S4 and S5 in PBS.

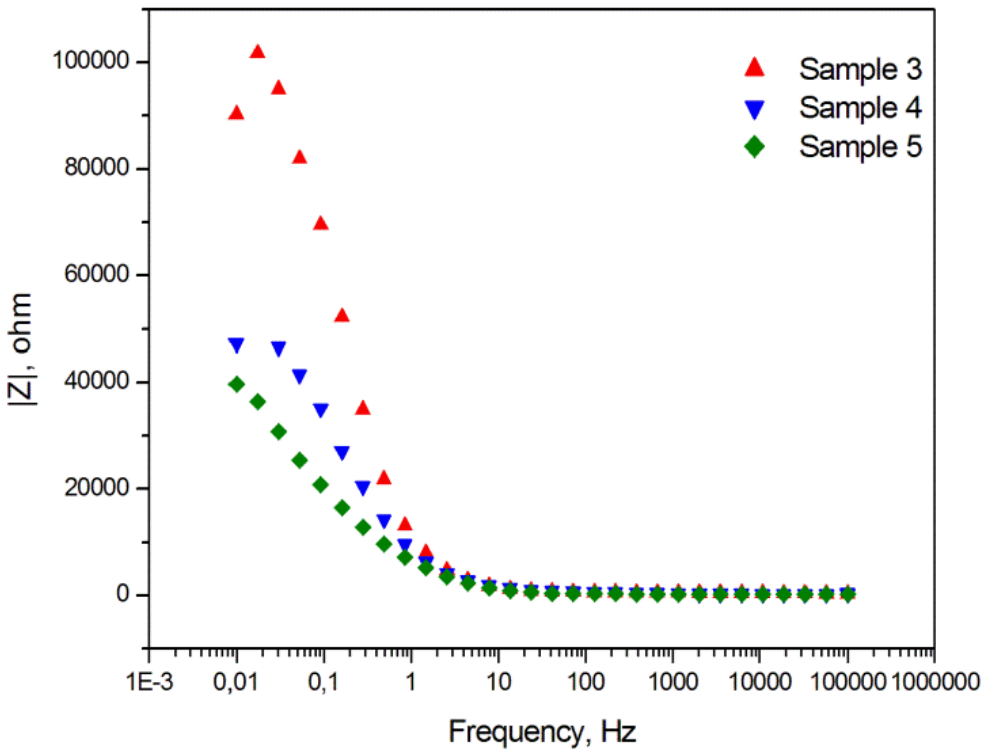

Figure 4.12: Bode Magnitude plot of samples S3, S4 and S5 in PBS.

Table 4.3: Equivalent circuit modeling for samples **S3**, **S4** and **S5** in PBS.

Sample	R_{sol} ($\Omega.cm^{-2}$)	Q_{dl} ($\mu S.s^{-n}.cm^{-2}$)	n	Rct ($\Omega.cm^{-2}$)	Q_{dl} ($\mu S.s^{-n}.cm^{-2}$)	n
3	260.9	12.06	0.994	7545	4.415	0.701
4	272.6	20.82	0.654	688.5	22.22	0.866
5	305.4	21.81	0.892	332	73.16	0.656

Sample (Table continue)	R_{fib} ($\Omega.cm^{-2}$)	Q_{ITO} ($\mu S.s^{-n}.cm^{-2}$)	n	R_{ITO} ($\Omega.cm^{-2}$)	χ^2
3	$9.55.10^4$	186.30	0.263	558	$4.683.10^{-4}$
4	$6.16.10^4$	–	–	–	$7.786.10^{-4}$
5	$3.879.10^4$	–	–	–	$3.211.10^{-4}$

As seen from the results, the specific capacitance was on the same order at about ~1.0 mF, with no apparent effect of the CTAB content on the total capacitance. Also the EIS results showed that the charge transfer resistance was related with the CTAB content. Fiber diameters and charge transfer resistances were found to decrease with the salt content, while the antibacterial activity and the double layer capacitance increased, because the fiber structure degraded and permitted the bromide ions to dissolve into the solution. The reduction in the charge transfer resistance was related to the change in fiber diameter and in consequence the surface area.

The simulated equivalent circuit model created with the ZSimpWin (version 3.10) software was compared with the experimental results obtained from the Nyquist and Bode magnitude plots (Rs, Cdl and Rct) and the results were shown in Table 4.3. R_{sol} showed the solution resistance, Qdl and Rct corresponded to the double layer phase element at the electrode surface and charge transfer resistance at the solution interface, respectively. Q_{fib}, R_{fib}, Q_{ITO} and R_{ITO} showed the fiber phase element, the fiber resistance the ITO electrode phase element and the ITO resistance respectively.

The results showed an R_{sol} ($Q_{dl}R_{ct}$ ($Q_{fib}R_{fib}$)) ($Q_{ITO}R_{ITO}$) equivalent circuit model as shown in Figure 4.13 with a χ^2 defined as the sum of the squares of the residuals and was minimized to an 10^{-4} error in PBS (Figure 4.13).

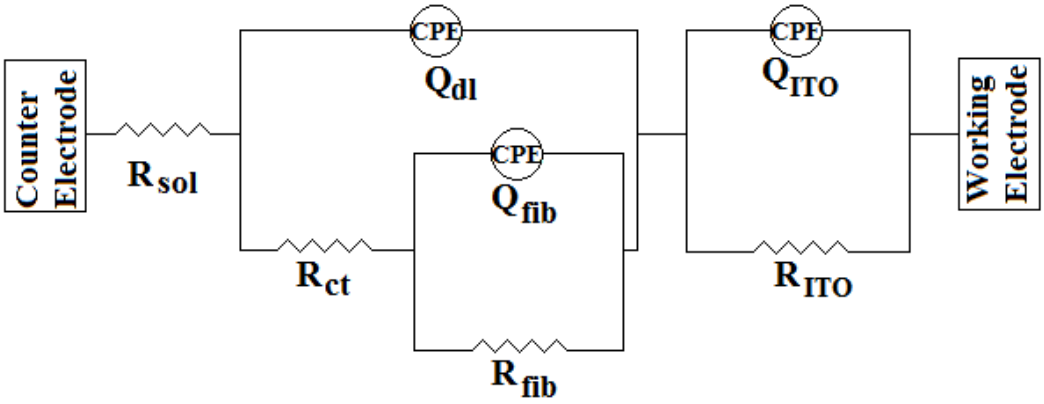

Figure 4.13: Schematical representation of the equivalent circuit modelling.

5. RESULTS AND DISCUSSIONS OF PVP/CPC

5.1 Morphological Analysis of PVP/CPC

PVP/CPC ratios (%wt/vol) of different nanofibrous web samples and their corresponding average fiber diameters are presented in Table 5.1. To determine the average fiber diameters, fifty measurements were taken from each sample and then the average values were calculated. SEM micrographs of five different samples containing different PVP/CPC ratios can be seen in Figure 5.1. As seen from Figure 5.1a, the PVP nanofibers have a smooth surface with a diameter range of 555 ±86 nm. The micrographs of PVP/CPC blends (Figure 5.1 b-e) demonstrate the presence of CPC salt in the form of crystalline particles clearly visible on the fibers. The introduction of CPC salt into the nanofibers affected the fiber morphology by a decrease in the average fiber diameter of PVP/CPC samples ranging from ~500 nm to ~200 nm compared to that of the pristine PVP samples without salt (Figure 5.2).

Table 5.1: PVP and CPC ratios (wt/v) of 5 different nanofibrous web samples

Sample No	PVP (%wt/v)	CPC (%wt/v)	Fiber diameter (nm)
S1C (control)	10.0	0.00	555 ± 86
S2C	10.0	0.5	292 ± 64
S3C	10.0	1.0	272 ± 92
S4C	10.0	2.5	256 ± 90
S5C	10.0	5.0	287 ± 75

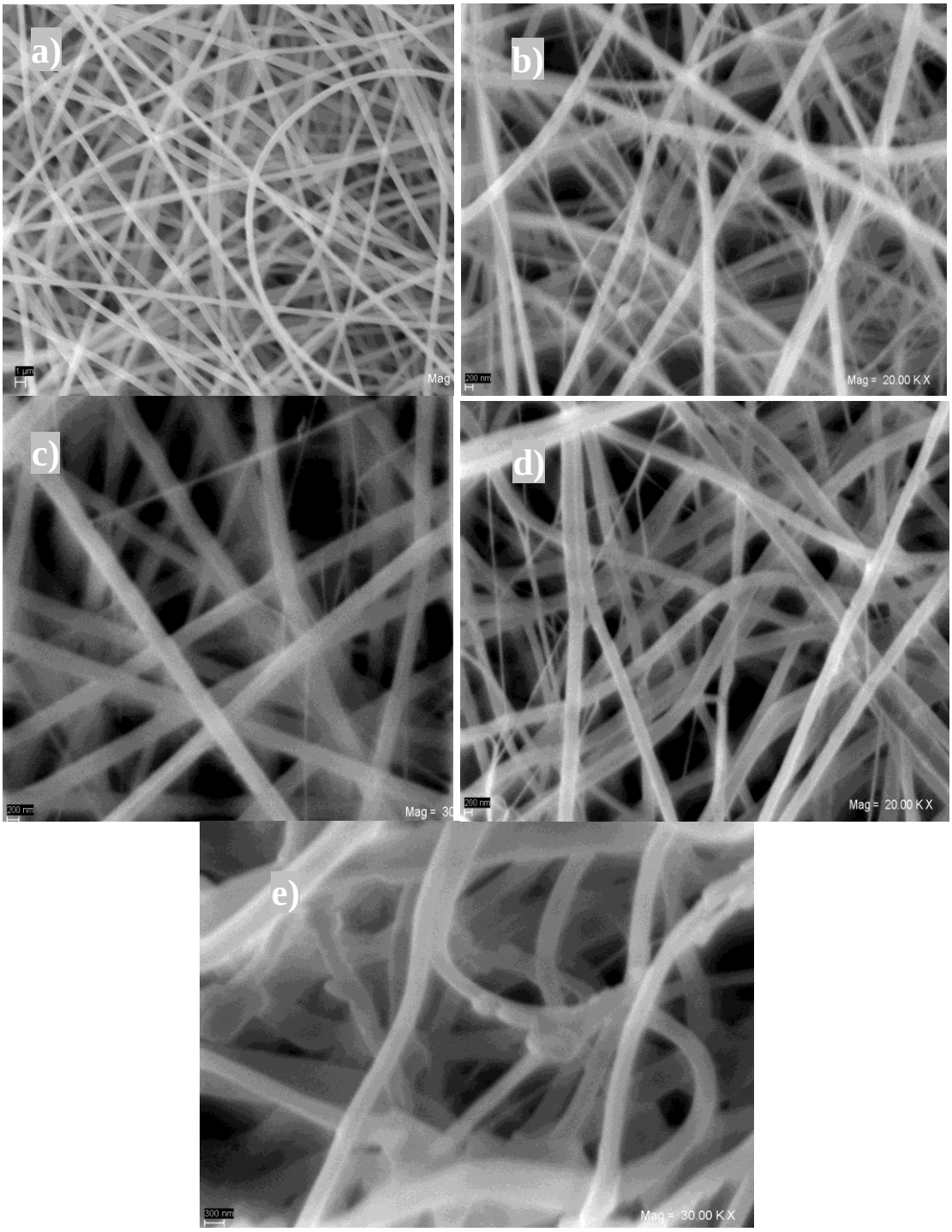

Figure 5.1: SEM micrographs of PVP/CPC nanofibers; a) S1C, b) S2C, c) S3C, d) S4C, e) S5C

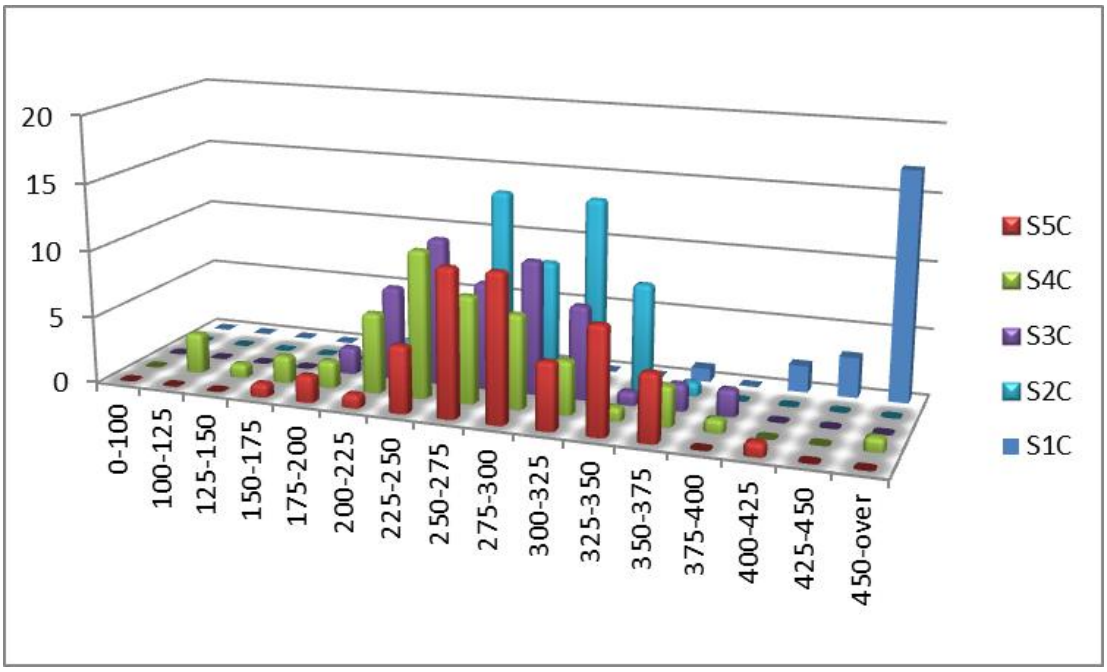

Figure 5.2: Fiber diameter distribution for the samples S1C through S5C.

5.2 FTIR-ATR Analysis of PVP/CPC

As can be seen from the FTIR absorbance spectrum in Figure 5.3, PVP and CPC possessed common peaks. The bands with peak locations at 2825 and 2875 cm^{-1} existed due to the C-H stretching of the ring CH groups on the side chains. In addition, a series of bands at 1450 cm^{-1} were attributed to the C=C bond (stretching) of the aromatic rings. Bands with peak locations at 750 cm^{-1} (out-of-plane) and 690 cm^{-1} (in-plane) due to the H–C bonds were visible for both PVP and CPC. The sharp peak at 2900 cm^{-1} corresponding to the C-H stretching vibration of the CH_2 and CH groups on the main chain are characteristic for CPC. Also the characteristic peaks for PVP existed at 1655cm^{-1} corresponding to the C=O stretching of the aromatic ring, and at 1285 cm^{-1} and 1500 cm^{-1} due to the C-N bonds and C-H bending, respectively. The absorbance (A) was found to increase with the increase in CPC content as seen in Figure 5.3.

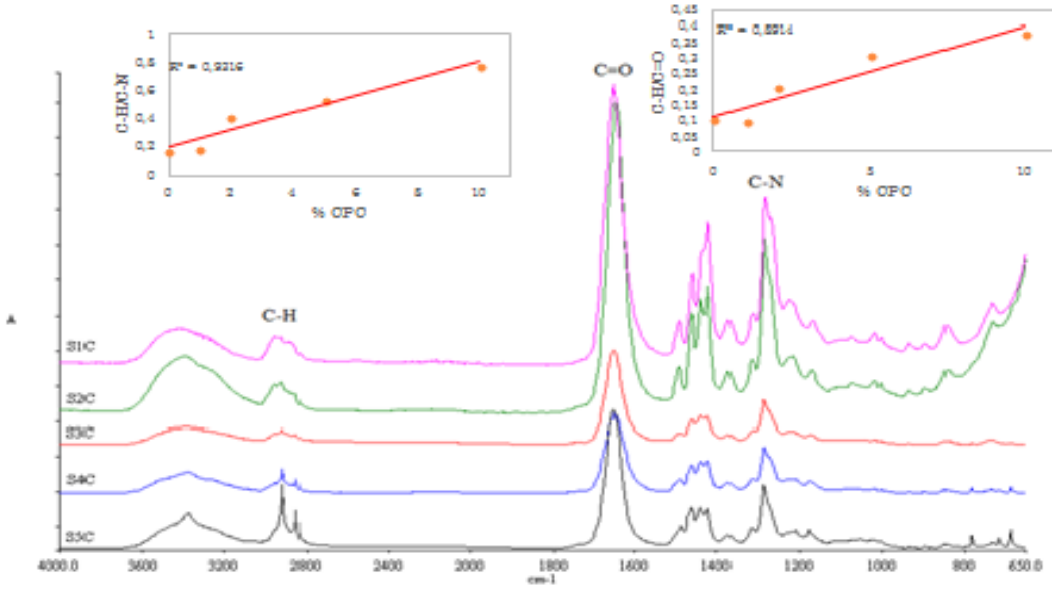

Figure 5.3: FTIR-ATR analysis of PVP/CPC samples; a)S1C, b)S2C, c)S3C, d)S4C, e)S5C. Inset: C-H/C=O and C-H/C-N ratios.

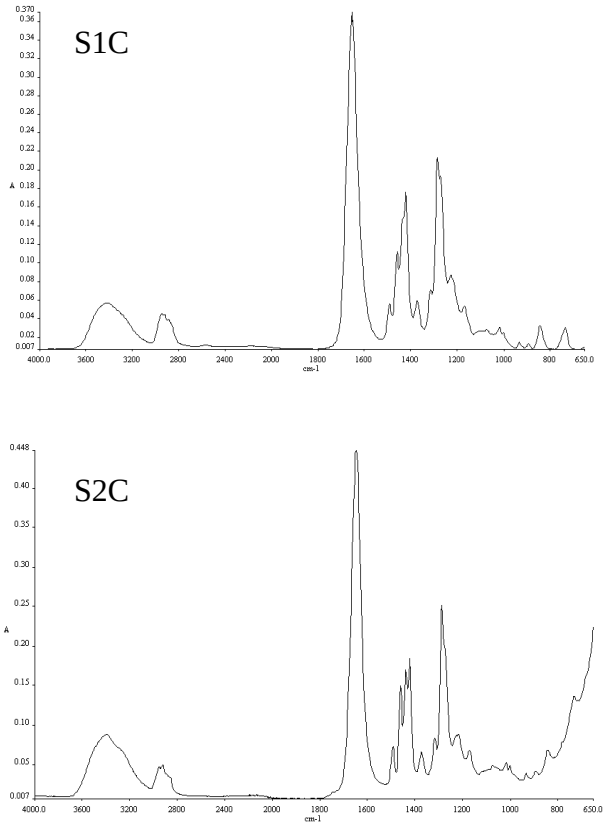

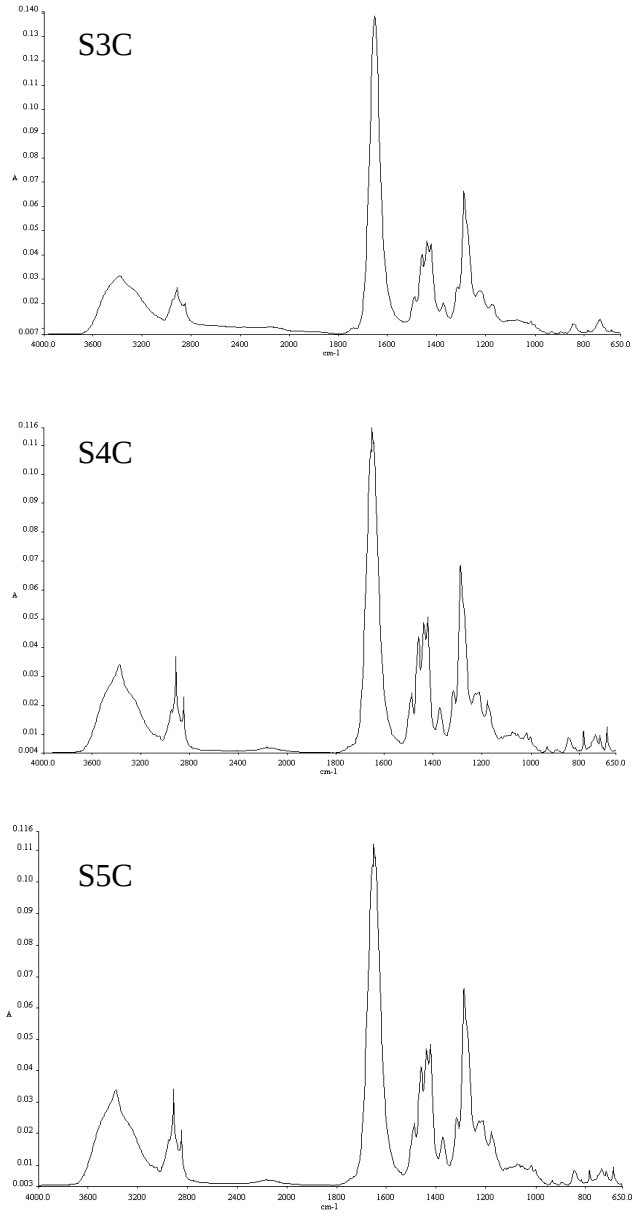

Figure 5.4: FTIR-ATR analysis of S1C-S5C, separately

5.3 Electrochemical Impedance Spectroscopy (EIS) Analysis of PVP/CPC

The electrochemical activity of the Cl ions, incorporated to the nanofibrous samples by the CPC presence, was determined using electrochemical impedance spectroscopy (EIS) method. PVP and PVP/CPC nanofiber coated ITO electrodes were used for EIS measurements and the results are shown in Figures 5.5-5.7. The electrodes were thermally cured for 24 hours at 150^{o}C to obtain a crosslinked PVPP. EIS measurements were conducted at a 20mV frequency band according to open circuit potential where the fiber surface was not harmed during the analysis. An ITO-PET

electrode surface was used to determine the electroactivity of CPC, PVP and the solvent. The measurements were done in a phosphate buffer solution (PBS) but in contrast to CTAB, the CPC samples dissolved instantaneously. As seen from the Nyquist diagram in Figure 5.5, the fiber electrodes consisted of a double semi-circular structure. The first semicircle was related to the double layer capacitance (C_{dl}) and the charge transfer resistance (R_{ct}). The second semicircle was related to the electrode behavior, depending on the CPC content and the preparative conditions of the fiber. Specific capacitance values were calculated via the formula $C_{sp} = 1 / 2\pi fZ''$ where C_{sp} shows the specific capacitance, f the frequency in Hz and Z'' the imaginary value at that point.

At 10 mHz frequency, samples S3C, S4C and S5C showed specific capacitance values of 100.7 $mF.cm^{-2}$, 13.7 $mF.cm^{-2}$ and 14.0 $mF.cm^{-2}$, respectively. Bode magnitude plot is used to determine the double-layer capacitance Cdl by extrapolating a line to log Z axis at $\omega = 1$ Hz yielding the value of Cdl by the relationship: $|Z| = 1 / C_{dl}$.

The double layer constant phase element Q_{dl} was found to increase with CPC content, being 34.15 $\mu S.s^{-n}.cm^{-2}$, 30.96 $\mu S.s^{-n}.cm^{-2}$ and 62.21 $\mu S.s^{-n}.cm^{-2}$ for the samples S3C, S4C and S5C, respectively, while the charge transfer resistance decreased stepwise from 526 $\Omega.cm^{-2}$ to 118 $\Omega.cm^{-2}$. On the other hand, the Bode phase plot phase angle approaches to a plateau in the frequency region of 1 Hz–10 Hz having a value standing between 55-60° with the CPC content.

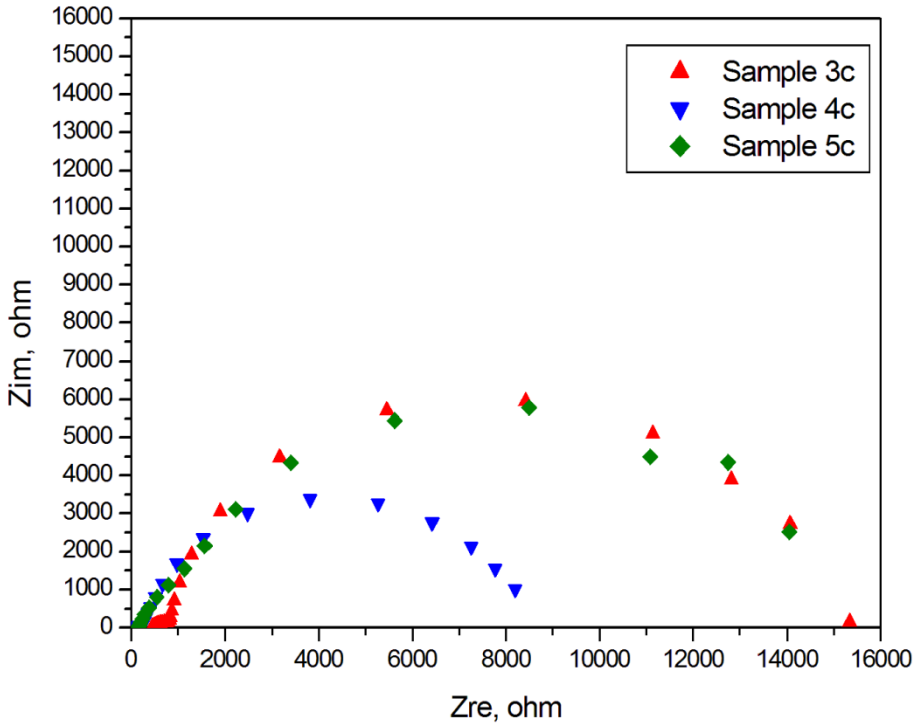

Figure 5.5: Nyquist plot of samples S3C, S4C and S5C in PBS.

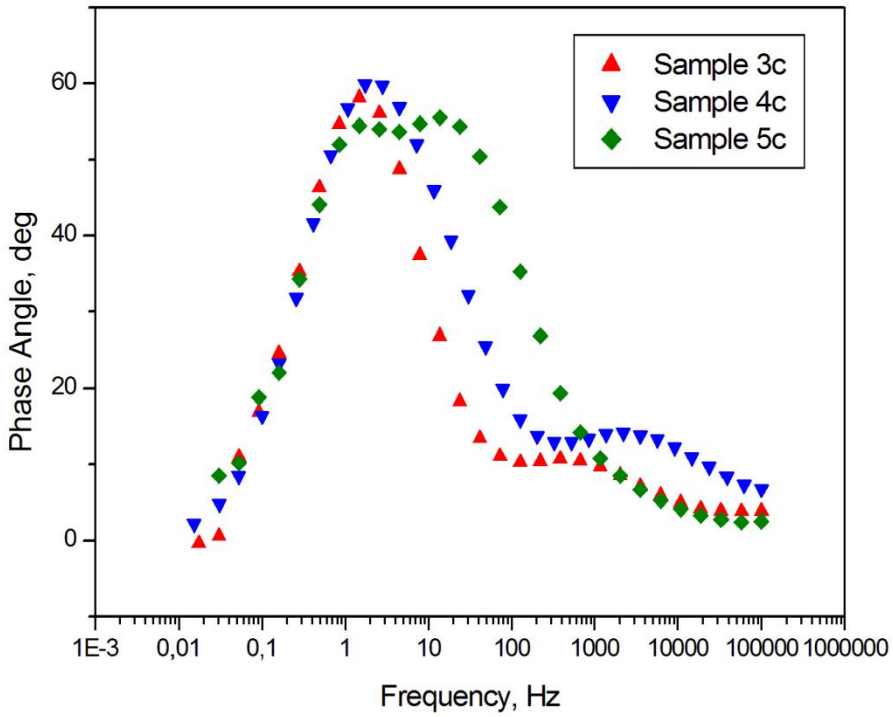

Figure 5.6: Bode Phase plot of samples S3C, S4C and S5C in PBS.

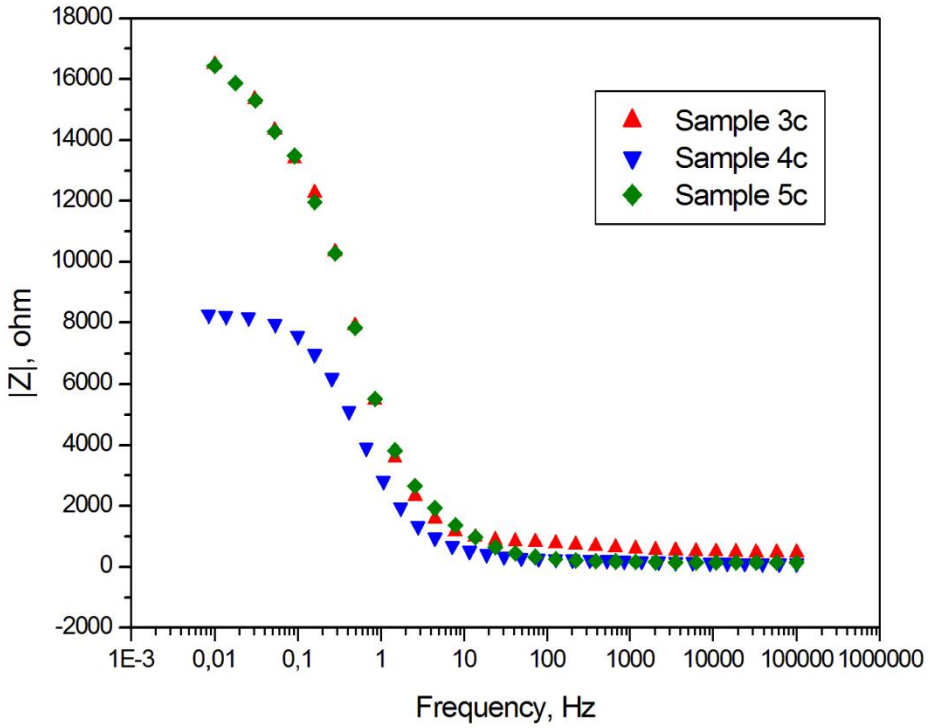

Figure 5.7: Bode Magnitude plot of samples S3C, S4C and S5C in PBS.

Table 5.2: Equivalent circuit modeling for samples **S3C**, **S4C** and **S5C** in PBS.

Sample	R_{sol} ($\Omega.cm^{-2}$)	Q_{dl} ($\mu S.s^{-n}.cm^{-2}$)	n	Rct ($\Omega.cm^{-2}$)	C_{fib} ($\mu S.s^{-n}.cm^{-2}$)	R_{fib} ($\Omega.cm^{-2}$)
3C	87.94	34.15	0.543	526	118.16	5619
4C	101.6	30.96	0.586	178.5	37.82	8542
5C	135	62.15	0.636	118	3.56	3860

Sample (Table continue)	C_{ITO} ($\mu S.s^{-n}.cm^{-2}$)	R_{ITO} ($\Omega.cm^{-2}$)	χ^2
3C	224	8434	$9.393.10^{-4}$
4C	68	139	$1.826.10^{-4}$
5C	56	$1.02.10^{4}$	$6.211.10^{-4}$

As seen from the results, the specific capacitance was varying from ~100.0 mF and 14 mF, with a decrease by increasing CPC content. The EIS results also showed that the charge transfer resistance was in close relation with the CPC content. Fiber diameters and charge transfer resistances were found to decrease with the salt content, while the antibacterial activity and the double layer capacitance increased. Although the double layer capacitance and charge transfer resistance were closely dependant with the CPC content in the fiber, the Rfib and Cfib values were on first found to change randomly with the CPC content. The fiber dissolved in PBS and permitted the chloride and quaternized ammonium ions to dissolve into the solution and increasing the conductivity of the solution. However, after a closer view the solubility of the fiber was independant with the CPC content but dependant with fiber diameters as seen in Figure 5.2. As a result, the capacitance (Cfib) and Rfib decreased with the increase of fiber diameter.

The simulated equivalent circuit model created with the ZSimpWin (version 3.10) software was compared with the experimental results obtained from the Nyquist and Bode magnitude plots (Rs, Cdl and Rct) and the results were shown in Table 5.2. R_{sol} showed the solution resistance, Qdl and Rct corresponded to the double layer phase element at the electrode surface and charge transfer resistance at the solution interface, respectively. The results showed an R_{sol} ($Q_{dl}R_{ct}$ ($Q_{fib}R_{fib}$)) ($Q_{ITO}R_{ITO}$) equivalent circuit model as shown in Figure 5.8 with a χ^2 defined as the sum of the squares of the residuals and was minimized to an 10^{-4} error in PBS.

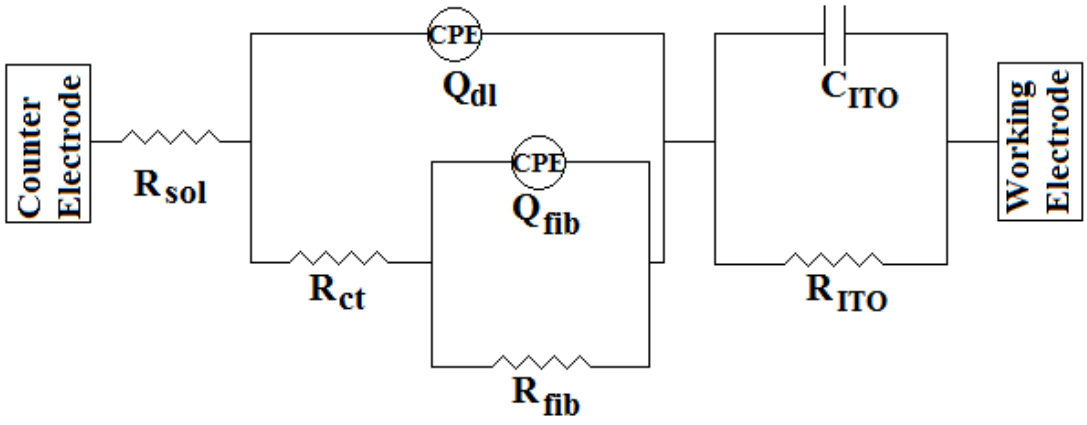

Figure 5.8: Schematical representation of the equivalent circuit modelling.

6. CONCLUSION

This study has pursued to fabricate antibacterial nanofibers with high porosity and flexibility that could be used in biomedical applications. For this purpose, porous PVP fibers incorporated with quaternary ammonium salts were obtained by electrospinning method.

There were many difficulties that had to be overcome during the preperations of the nano scaled fibers. The primary problem was that the salts incorporated into the spinning solution rendered a lower viscosity and an increase in the crystallinity of the obtained fibers which hinders a decent morphology. The second concern was about that the surrounding conditions such as the quality of the air, the current flow, the humidty etc. affected the electrospinability of the solution mixture. Moreover, a way to optimize electrospinning conditions without the occurance of beads at high salt amounts could not be resolved.

We worked on four different quaternary ammonium salts during this study. Cetyltrimethylammonium bromide (CTAB), cetylpyrridinium chloride (CPC), hexadecyltrimethylammonium chloride (HTAC) and dodecyltrimethylammonium bromide (DTAB) were investigated for a homogeneous dispersion, a good morphology and high antibacterial activity even at low concentrations. Only two of them CTAB and CPC were able to produce fibers with a better shaped morphology. The other ones were not compatible with PVP and environmental friendly non-toxic alcohol (Ethyl alcohol) based solvent systems to obtain decent fibers for biomedical applications.

A comparative study was also pursuited between CPC and CTAB based on those nanofibers. The morphological analysis between CPC and CTAB revealed that CTAB incorporated nanofibers were more convenient regarding to CPC with less beads and errors in the fiber morphology (Figure 4.1 and Figure 5.1). CPC salt illustrates some errors and beads in the fiber morphology, especially with the increasing amounts of CPC (Figure 5.1 e). Therefore, CTAB salt has been found more appropriate for our purpose in this project which has been proved with the morphological analysis and FTIR analysis.

FTIR spectrums of CPC and CTAB have similarity between each other, with only a few specific differences in the intensities. PVP/CTAP peak ratios show better linearity compared to PVP/CPC peak ratios. The morphology of the fibers also proved that PVP/CPC does not show such an accordance as it is in PVP/CTAB.

The EIS measurements showed that charge transfer resistance is decreasing with the increasing salt amounts for both CTAB and CPC. This result approve that the solution and electrode interface conductivity is closely related with the salt content in the fiber structure. But, on the other hand the fiber conductivity reciprocally related to R_{fib} seems to be better for CPC samples. This could be explained by the fact that PVP/CTAB fibers electrospun on ITOPET dissolved less than PVP/CPC fibers on ITOPET in PBS solution. As known, the thickness of the fiber on ITOPET surface also affects the conductivity values. This result could also explain why the Rct values are lower for CPC samples according to CTAB samples. Because, the dissolved CPC ions increase the conductivity of the solution while lowering the charge transfer resistance.

REFERENCES

[1] **Pant, H.R., Bajgai, M.P., Nam, K.T., Seo, Y.A., Pandeya, D.R., Hong, S.T., Kim H.K.** (2011). Electrospun nylon-6 spider-net like nanofiber mat containing TiO_2 nanoparticles: a multifunctional nanocomposite textile material, *Journal of Hazardous Materials*, 185, 124.

[2] **Hong, K.H.** (2007). Preparation and properties of electrospun poly (vinyl alcohol)/silver fiber web as wound dressings, *Polymer Engineering and Science*, 47(1), 43.

[3] **Risbud, M.V., Bhat, S.V.,** (2001). Silver nanoparticles dispersed in electrospun polyacrylonitrile nanofibers via chemical reduction, *Journal of Materials Science: Materials in Medicine*, 12, 75.

[4] **Lee, D. Y., Lee, K.H., Kim, B.Y., Cho, N.I.,** (2010). Silver nanoparticles dispersed in electrospun polyacrylonitrile nanofibers via chemical reduction, *Journal of Sol-Gel Science and Technology*, 54, 63.

[5] **Wu, Y., Jia, W., An, Q., Liu, Y., Chen, J., Li, G.** (2009). Multiaction antibacterial nanofibrous membranes fabricated by electrospinning: an excellent system for antibacterial applications, *Nanotechnology*, 20, 245101.

[6] **Sheikh, F.A., Barakat, N.A.M., Kanjwal, M.A., Chaudhari, A.A., Jung, I.H., Lee, J.H., Kim, H.Y.** (2009). Electrospun antimicrobial polyurethane nanofibers containing silver nanoparticles for biotechnological applications, *Macromolecular Research*, 17, 9, 688.

[7] **Zhuang, X., Cheng, B., Kang, W., Xua, X.** (2010). Electrospun chitosan/gelatin nanofibers containing silver nanoparticles, *Carbohydrate Polymers*, 82, 524.

[8] **Zahedi, P., Rezaeian, I., Ranaei-Siadat, S. O., Jafari, S.H., Supaphol, P.** (2010). Surface modification and antibacterial activity of electrospun

polyurethane fibrous membranes with quaternary ammonium moieties, *Polymers for Advanced Technologies*, 21 (2), 77.

[9] **Yao, C., Li, X., Neoh, K.G., Shi, Z., Kang, E.T.** (2008). Surface modification and antibacterial activity of electrospun polyurethane fibrous membranes with quaternary ammonium moieties, *Journal of Membrane Science*, 320, 259.

[10] **Barnabas, J., Miraftab, M., Qinand, Y., Changjun, Z.** (2013). Evaluating the antibacterial properties of chitosan fibres embedded with copper ions for wound dressing applications, *Journal of Industrial Textiles*

[11] **Kenawy, E.R., Abdel-Hay, F.I., El-Magd, A.A., Mahmoud, Y.** (2006). Biologically active polymers: VII. Synthesis and antimicrobial activity of some crosslinked copolymers with quaternary ammonium and phosphonium groups, *Reactive & Functional Polymers*, 66, 419.

[12] **Jeon, H.J., Kim, J.S., Kim, T.G., Kim, J.H., Yu, W.R., Youk, J.H.** (2008). Preparation of poly (ε-caprolactone)-based polyurethane nanofibers containing silver nanoparticles, *Applied Surface Science*, 254, 5886.

[13] **Dong, G., Xiao, X., Liu, X., Qian, B., Liao, Y., Wang, C., Chen, D., Qiu, J.** (2009). Functional Ag porous films prepared by electrospinning, *Applied Surface Science*, 255, 7623.

[14] **Goel, N.K., Rao, M.S., Kumar, V., Bhardwaj, Y.K., Chaudhari, C.V., Dubey, K.A., Sabharwal, S.** (2009). Synthesis of antibacterial cotton fabric by radiation-induced grafting of [2-(Methacryloyloxy) ethyl] trimethylammonium chloride (MAETC) onto cotton, *Radiation Physics and Chemistry*, 78, 399.

[15] **Chang, H., Yang, M.S., Liang, M.** (2010). The synthesis, characterization and antibacterial activity of quaternized poly (2, 6-dimethyl-1, 4-phenylene oxide) s modified with ammonium and phosphonium salts, *Reactive & Functional Polymers*, 70, 944.

[16] **Hasan, J., Crawford, R.J., Ivanova, E.P.** (2013). Antibacterial surfaces: the quest for a new generation of biomaterials, *Trends in Biotechnology***,** 31 (5), 295.

[17] **Lee, K., Lee, S.** (2012). Multifunctionality of poly (vinyl alcohol) nanofiber webs containing titanium dioxide, *Journal of Applied Polymer Science*, 124, 4038

[18] **Jeong, E.H., Yang, J., and Youk, J.H.** (2007), Preparation of polyurethane cationomer nanofiber mats for use in antimicrobial nanofilter applications, *Materials Letters*, 61, 3991.

[19] **Park, I.K., Ihm, J.E., Park, Y.H., Choi, Y.J., Kim, S.I., Kim, W.J., Akaike, T., Cho, C.S.** (2003). Galactosylated chitosan (GC)-graft-poly(vinyl pyrrolidone) (PVP) as hepatocyte-targeting DNA carrier: Preparation and physicochemical characterization of GC-graft-PVP/DNA complex (1), *Journal of Controlled Release*, 86, 349.

[20] **Archana, D., Singh, B.K., Dutta, J., Dutta, P.K.** (2013). In vivo evaluation of chitosan–PVP–titanium dioxide nanocomposite as wound dressing material, *Carbohydrate Polymers*, 95, 530.

[21] **EI-Arini, S.K., Leuenberger, H.** (1995). Modelling of drug release from polymer matrices: Effect of drug loading, *International Journal of Pharmaceutics*, 121, 141.

[22] **Dorati, R., Genta, I., Colonna, C., Modena, T., Pavanetto, F., Perugini, P., Conti, B.** (2007). Investigation of the degradation behaviour of poly (ethylene glycol-co-d, l-lactide) copolymer, *Polymer Degradation and Stability*, 92, 1660.

[23] **Huang, L.Y., Branford-White, C., Shen, X.X., Yu, D.G., Zhu, L-M.** (2012). Time-engineeringed biphasic drug release by electrospun nanofiber meshes, *International Journal of Pharmaceutics*, 436, 88.

[24] **Kumar, V., Yang, T., Yang, Y.** (1999). Interpolymer complexation. I. Preparation and characterization of a polyvinyl acetate phthalate-polyvinylpyrrolidone (PVAP-PVP) complex, *International Journal of Pharmaceutics*, 188, 221.

[25] **Kaneda, Y., Tsutsumi, Y., Yoshioka, Y., Kamada, H., Yamamoto, Y., Kodaira, H., Tsunoda, S., Okamoto, T., Mukai, Y., Shibata, H., Nakagawa, S., Mayumi, T.**. (2004). The use of PVP as a polymeric

carrier to improve the plasma half-life of drugs, *Biomaterials*, 25, 3259.

[26] **Singh, B., Pal, L.** (2011). Radiation crosslinking polymerization of sterculia polysaccharide–PVA–PVP for making hydrogel wound dressings, *International Journal of Biological Macromolecules*, 48, 501.

[27] **Son, W.K., Youk, J.H., and Park W.H.** (2006). Antimicrobial cellulose acetate nanofibers containing silver nanoparticles, *Carbohydrate Polymers*, 65, 430.

[28] **Martins, N.C.T., Freire, C.S.R., Neto, C.P., Silvestre, A.J.D., Causio, J., Baldi, G., Sadocco, P., Trindade, T.** (2013). Antibacterial paper based on composite coatings of nanofibrillated cellulose and ZnO, *Colloids and Surfaces A: Physicochem. Eng. Aspects*, 417, 111.

[29] **Charernsriwilaiwat, N., Rojanarata, T., Ngawhirunpat, T., Sukma, M., Opanasopit, P.** (2013). Electrospun chitosan-based nanofiber mats loaded with Garcinia mangostana extracts, *International Journal of Pharmaceutics*, 452, 333.

[30] **Martins, N.C.T., Freire, C.S.R., Neto, C.P., Silvestre, A.J.D., Causio, J., Baldi, G., Sadocco, P., Trindade, T.** (2013). Antibacterial paper based on composite coatings of nanofibrillated cellulose and ZnO, *Colloids and Surfaces A: Physicochem. Eng. Aspects*, 417, 111.

[31] **Haaf, F., Sanner, A. And Straub, F.** (1985). Polymers of N-vinylpyrrolidone: synthesis, characterization and uses, *Polymer Journal*, 17(1): 143–152.

[32] **Bühler, Volker** (2005). Polyvinylpyrrolidone Excipients for Pharmaceuticals, *Berlin, Heidelberg, New York: Springer*. pp. 1–254.

[33] **Santhi Ganesan, M.D.** (2003). Embolized Crospovidone (poly N-vinyl-2-pyrrolidone) in the Lungs of Intravenous Drug Users, *Pathol*, 16(4):286–292.

[34] **Sibes Kumar Das, Samirendra Kumar Saha, Anirban Das, Arup Kumar Halder,Sourindra Nath Banerjee, Mukul Chakraborty** (2008). A study of comparison of efficacy and safety of talc and povidone iodine

for pleurodesis of malignant pleural effusions. *Journal of the Indian Medical Association*, 106 (9): 589–90, 592.

[35] **IUPAC,** *Compendium of Chemical Terminology*, 2nd ed. (the "Gold Book") (1997).

[36] **Smith, Michael B., March, Jerry.** (2001). *Advanced Organic Chemistry: Reactions, Mechanisms, and Structure* (5th ed.), New York: Wiley-Interscience.

[37] **Jia, Zhishen; Shen, Dongfeng; Xu, Weiliang.** (2001). Synthesis and antibacterial activities of quaternary ammonium salt of chitosan, *Carbohydrate Research*, 333 (1): 1–6.

[38] *Potential Use of Cetrimonium Bromide as an Apoptosis-Promoting Anticancer Agent for Head and Neck Cancer*, 76 (5): 969–983. Retrieved November 2009.

[39] **Asadoorian J, Williams KB,** (2008). Cetylpyridinium chloride mouth rinse on gingivitis and plaque, *Journal of Dental Hygiene*, 82 (5).

[40] **Ioannis S. Chronakis,** (2005). Novel nanocomposites and nanoceramics based on polymer nanofibers using electrospinning process—a review, *Journal of Materials Processing Technology*, 167, 283–293.

[41] **Deitzel, J.M., Kosik, W., McKnight, S.H., Tan, N.C.B., Desimone, J. M., Crette, S.** (2002). Electrospinning of polymer nanofibers with specific surface chemistry, *Polymer*, 43, 1025–1029.

[42] **Bognitzki, M., Hou, H., Ishaque, M., Frese, T., Hellwig, M., Schwarte, C., Shaper, A., Wendorff, J.H., Greiner, A.** (2000). Polymer, metal, and hybrid nano-and mesotubes by coating degradable polymer template fibers (TUFT process), *Adv. Mater.*, 12, 637–640.

[43] **Reneker, D.H., Yarin, A.L., Zussman, E., Xu, H.** (2007). Electrospinning of nanofibers from polymer solutions and melts, *Advances in applied mechanics*, Vol.41, 46.

[44] **Huanga, Z.M., Zhang, Y.Z., Kotaki, M., Ramakrishna, S.** (2003). A review on polymer nanofibers by electrospinning and their applications in nanocomposites, *Composites Science and Technology*, 63, 2223–2253.

[45] **Yarin, L.A., Koombhongse, S., Reneker, H.D.** (2001). Bending instability in electrospinning of nanofibers, *J Appl Phys*, 89, 3018–3026.

[46] **Adomaviciute, E., Rimvydas, M.** (2007). Methods of Forming Nanofibres from Bicomponent PVA/Cationic Starch Solution, *Fibers Text East Eur*, 15, 64–65.

[47] **Bhardwaj, N., Kundu, S.C.** (2010). Electrospinning: a fascinating fiber fabrication technique, *Biotechnology Advances*, 28, 325–347.

[48] **Chong, EJ., Phan, T.T., Lim, I.J., Zhang, Y.Z., Bay, B.H., Ramakrishna, S.** (2007). Evaluation of electrospun PCL/gelatin nanofibrous scaffold for wound healing and layered dermal reconstitution, *Acta Mater*, 3, 321–330.

[49] **Deitzel, J.M., Kleinmeyer, J., Harris, D., Beck Tan, N.C.** (2001). The effect of processing variables on the morphology of electrospun nanofibers and textiles, *Polymer*, 42(1):261–272.

[50] **Eda, G., Shivkumar, S.** (2007). Bead-to-fiber transition in electrospun polystyrene, *J Appl Polym Sci*, 106(1):475–487.

[51] **Yang, Q., Li, Z., Hong, Y., Zhao, Y., Qiu, S., Wang, C., Wei, Y**. (2004). Influence of solvents on the formation of ultrathin uniform poly (vinyl pyrrolidone) nanofibers with electrospinning, *J Polym Sci, Part B: Polym Phys*, 42(20):3721–3726.

[52] **Koski, A., Yim, K., Shivkumar, S.** (2004). Molecular weight dependent structural regimes during the electrospinning of PVA, *Materials Letters*, 58 (3–4):493–497.

[53] **Zhao, Y.Y., Yang, Q.B., Lu, X.F., Wang, C., Wei, Y.** (2005). Study on correlation of morphology of electrospun products of polyacrylamide with ultrahigh molecular weight, *J Polym Sci, Part B: Polym Phys*, 43(16):2190–2195.

[54] **Larrondo, L., St. John Manley, R.** (1981). Electrostatic fiber spinning from polymer melts. I. Experimental observations on fiber formation and properties, *J Polym Sci: Polym Phys Ed*, 19(6):909–920

[55] **Ding, B., Kim, H.Y., Lee, S.C., Shao, C.L., Lee, D.R., Park, S.J., Kwag, G.B., Choi, K.J.** (2002). Preparation and characterization of a nanoscale poly (vinyl alcohol) fiber aggregate produced by an

electrospinning method, *J Polym Sci, Part B: Polym Phys* 40(13):1261–1268.

[56] **Ki, C.S., Baek, D.H., Gang, K.D., Lee, K.H., Um, I.C., Park, Y.H.** (2005). Characterization of gelatin nanofiber prepared from gelatin–formic acid solution, *Polymer*, 46(14):5094–5102.

[57] **Kim, K.H., Jeong, L., Park, H.N., Shin, S.Y., Park, W.H., Lee, S.C., Kim, T.I., Park, Y.J., Seol, Y.J., Lee, Y.M., Ku, Y., Rhyu, I.C., Han, S.B., Chung, C.P.** (2005). Biological efficacy of silk fibroin nanofiber membranes for guided bone regeneration, *J Biotechnol*, 120(3):327–339.

[58] **Lee, J.S., Choi, K.H., Ghim, H.D., Kim, S.S., Chun, D.H., Kim, H.Y., Lyoo, W.S.** (2004). Role of molecular weight of atactic poly (vinyl alcohol)(PVA) in the structure and properties of PVA nanofabric prepared by electrospinning, *J Appl Polym Sci*, 93(4):1638–1646.

[59] **Zhang, Y., Ouyang, H., Lim, C.T., Ramakrishna, S., Huang, Z.M.** (2005). Electrospinning of gelatin fibers and gelatin/PCL composite fibrous scaffolds, *J Biomed Mater Res Part B: Appl Biomater*, 72(1):156–165.

[60] **Fong, H., Chun, I., Reneker, H.D.** (1999). Beaded nanofibers formed during electrospinning, *Polymer*, 40, 4585–92.

[61] **Zhang, C., Yuan, X., Wu, L., Han, Y., Sheng, J.** (2005). Study on morphology of electrospun poly (vinyl alcohol) mats, *Eur Polym J***,** 41, 423–32.

[62] **Pham, P.Q., Sharma, U., Mikos, G.A.** (2006). Electrospun poly (ε-caprolactone) microfiber and multilayer nanofiber/microfiber scaffolds: characterization of scaffolds and measurement of cellular infiltration, *Biomacromolecules*, 7, 2796–2805.

[63] **Sukigara, S., Gandhi, M., Ayutsede, J., Micklus, M., Ko, F.** (2003). Regeneration of Bombyx mori silk by electrospinning—part 1: processing parameters and geometric properties, *Polymer*, 44, 5721-7.

[64] **Zong, X., Kim, K., Fang, D., Ran, S., Hsiao, B.S., Chu, B.** (2002). Structure and process relationship of electrospun bioabsorbable nanofiber membranes, *Polymer*, 43(16):4403–4412.

[65] **Huang, C., Chen, S., Lai, C., Reneker Darrell, H., Qiu, H., Ye, Y., Hou, H.** (2006). Electrospun polymer nanofibres with small diameters, *Nanotechnology*, 17(6):1558–1563.

[66] **Taylor, G.** (1964). Disintegration of Water Drops in an Electric Field, Proc. R. Soc. Lond., vol.280, pp. 383-397

[67] **Zhong, X.H., Kim, K.S., Fang, D.F., Ran, S.F., Hsiao, B.S. and Chu, B.** (2002). Structure and process relationship of electrospun bioabsorbable nanofiber membranes, *Polymer*, vol.43, pp. 4403-4412

[68] **Deitzel, J.M., Kosik, W., McKnight, S.H., Tan, N.C.B., DeSimone, J.M. and Crette, S.** (2002). *Polymer*, 43, 1025-1029

[69] **Jarusuwannapoom, T., Hongrojjanawiwat, W., Jitjaicham, S., Wannatong, L., Nithitanakul, M., Pattamaprom, C., Koombhongse, P., Rangkupan, R., Amd Supaphol, P.** (2005). Effect of solvents on electro-spinnability of polystyrene solutions and morphological appearance of resulting electrospun polystyrene fibers, *Euro. Polym. J.*, 41, 409-421

[70] **Wang, C., Hsu, C.H. and Lin, J.H.** (2006). *Macromolecules*, 39, 7662-7672

[71] **Baker, S.C., Atkin, N., Gunning, P.A., Granville, N., Wilson, K., Wilson, D., Southgate, J.** (2006). Characterisation of electrospun polystyrene scaffolds for three-dimensional in vitro biological studies, *Biomaterials*, 27, 3136-6146

[72] **Yuan, X.Y., Zhang, Y.Y., Dong, H.C., Sheng, J.** (2004). Morphology of ultrafine polysulfone fibers prepared by electrospinning, *Polym Int*, 53, 1704–10.

[73] **Megelski, S., Stephens, J.S., Chase, D. B., Rabolt, F.J.** (2002). Micro-and nanostructured surface morphology on electrospun polymer fibers, *Macromolecules*, 35, 8456–66.

[74] **Zong, X., Kim, K., Fang, D., Ran, S., S. Hsiao, B., Chu, B.** (2002). Structure and process relationship of electrospun bioabsorbable nanofiber membranes, *Polymer*, 439, 4403-12.

[75] **Megelski, S., Stephens, J.S., Chase, D.B. and Rabolt, J.F.** (2002). Micro-and nanostructured surface morphology on electrospun polymer fibers, *Macromolecules*, 35, 8456-8466.

[76] **Wang, C., Hsu, C.H. and Lin, J.H.** (2006). Scaling laws in electrospinning of polystyrene solutions, *Macromolecules*, 39, 7662-7672.

[77] **Wang, X., Um, C.I., Fang, D., Okamoto, A., Hsiao, S.B., Chu, B.** (2005). Formation of water-resistant hyaluronic acid nanofibers by blowing-assisted electro-spinning and non-toxic post treatments, *Polymer*, 46, 4853–67.

[78] **Cetiner, S., Kalaoglu, F., Karakas, H., Sarac**, **A.S.** (2010). Electrospun nanofibers of polypyrrole-poly (acrylonitrile-co-vinyl acetate), *Textile Research Journal*, 80, 1784-1792.

[79] **Macdolnald, J.R.** (1997). Impedance spectroscopy, John Wiley and Sons, New York.

[80] **Lang, G. and Inzelt, G.** (1991). Some problems connected with impedance analysis of polymer film electrodes: effect of the film thickness and the thickness distribution, *Electrochimica acta*, 36, 847-854.

[81] **D'Errico, G., De Lellis, M., Mangiapia, G., Tedeschi, A., Ortona, O., Fusco, S., Borzacchiello, A., Ambrosio, L.** (2008). Structural and mechanical properties of UV-photo-cross-linked poly (N-vinyl-2-pyrrolidone) hydrogels, *Biomacromolecules*, 9(1), 231.

[82] **Lopergolo, L.C., Lugao, A.B., Catalani, L.H.** (2003). Direct UV photocrosslinking of poly(*N*-vinyl-2-pyrrolidone) (PVP) to produce hydrogels, *Polymer*, 44, 6217.

[83] **Fechine, G.J.M., Barros, J.A.G., Catalani, L.H.** (2004). Poly(*N*-vinyl-2-pyrrolidone) hydrogel production by ultraviolet radiation: new methodologies to accelerate crosslinking, *Polymer*, 45, 4705.

[84] **Mirdamadi-Esfahani, M., Lampre, I., Marignier, J.L., de Waele, V., Mostafavi, M.** (2009). Radiolytic formation of tribromine ion Br_3^- in aqueous solutions, a system for steady-state dosimetry, *Radiation Physics and Chemistry*, 78, 106

CURRICULUM VITAE

Name – Surname: Nurullah UYKUN

Place and Date of Birth: ISTANBUL / 01.01.1989

Address: Baris Mah Fidangor Cad No: 3/17 34520 Beylikduzu, ISTANBUL

E-mail: nuykun1989@gmail.com

BSc: Karadeniz Technical University – Chemistry (2012)

Fellowships:

Ghent University (February 2014 – June 2014)

Publications:

1) N. Uykun, I. Ergal, H. Kurt, A. Gokceoren, I. Gocek, B. Kayaoglu, A. Akarsubasi, A. Sarac, "Electrospun Antibacterial Nanofibrous Polyvinylpyrrolidone/ Cetyltrimethylammonium Bromide Membranes for Potential Biomedical Applications", 2014, Journal of Bioactive and Compatible Polymers (in press)

Presentations:

1) European Polymer Federation (EPF2013) Congress Pisa, Italy, June 16-21, 2013 (Poster Presentation)

2)10th International Electrochemistry Meeting, Konya, Turkey, September 4-8, 2013 (Poster Presentation)